SILICA COATED IRON OXIDE NANOPARTICLES FOR ENVIRONMENT REMEDIATION AND NUCLEAR WASTE MANAGEMENT

Report submitted in partial fulfillment of the requirements of the degree of

European Master in Nuclear Energy (EMINE)

By

Md Al Mamun
2019-2020 M2 EMINE

Research Laboratory

Materials Science Division
Atomic Energy Centre Dhaka
Bangladesh Atomic Energy Commission

Supervisor

Dr. Engr. Sheikh Manjura Hoque
E-mail: **manjura_hoque@yahoo.com**
Materials Science Division, Atomic Energy Centre
4, Kazi Nazrul Islam Avenue, P.O. Box-164, Ramna,
Dhaka-1000, Bangladesh

Academic Mentor

Dr. Luc Salvo
Grenoble INP PHELMA, France

Acknowledgement

I would like to take the privilege to express my gratitude and deep respect to my supervisor Dr. Engr. Sheikh Manjura Hoque, Head and Chief Scientific Officer, Materials Science Division, Atomic Energy Centre Dhaka (AECD), Bangladesh Atomic Energy Commission, for her excellent guidance, expert advice, continuous cooperation and encouragement for carrying out the difficult work and preparation of the thesis. I will be ever grateful for her enormous help to complete my thesis work.

I would like to express my deepest and heartfelt of gratitude and honor to my respected teachers and academic mentors Dr. Luc Salvo and Dr. Emilie Ferrie, Professors, Grenoble INP Phelma, Grenoble, France and Program Directors, European Master in Nuclear Energy (EMINE), for their valuable academic as well as organizational guidance and advice. I also thank them and the whole team of EMINE program for their unending support and help throughout my EMINE master journey.

I am very grateful to all scientists of Materials Science Division, AECD, specially Dr. Md. Mahbubul Haque, Principal Scientific Officer, Dr. Md. Al-Mamun, Senior Scientific Officer, Dr. Harinarayan Das, Senior Scientific Officer, Dr. Rimi Rashid, Senior Engineer for giving me necessary supports to carry out the works whenever I needed.

I am specially grateful to Anjuman Ara Begum, Experimental Officer, Nazmunnahar Begum, Research Assistant and Jharna Begum, Scientific Assistant for their special help throughout my work and also thankful to all other members and staffs of Materials Science Division, AECD.

Finally, I give my respects and love to my parents and family members for their support, sacrifices and encouragement.

Forever Grateful
Md. Al Mamun.

Contents

List of Figures

List of Tables

Abstract

Environmental contamination, specially water pollution by toxic heavy metals and radionuclides from both natural and artificial sources is a big concern all over the world. Groundwater, Irrigation water and river water pollution by heavy metals mainly coming from industrial sources is also a big problem for Bangladesh. Nanomaterials specially magnetite iron oxide nanoparticles (MNP) are recently gained much interest in biomedical, environmental and nuclear application for its high surface area, adsorption capacity and excellent superparamagnetic properties. To prevent agglomeration, dissolution and leaching of magnetite in aqueous and highly acidic conditions, surface modification of magnetite nanoparticles by silica coating or formation of magnetite-silica core shell structure gained much popularity among the researchers. Silica coating, not only protects the magnetite core but also provides easy conjugation with different application specific functional groups and higher adsorption capacity. In this work, Silica coated magnetic nanoparticles (SMNP) were prepared by optimized and simplified methods using the available lab facilities. Chemical, Structural and Magnetic properties of uncoated and coated samples were characterized and measured by Fourier Transforms Infrared Spectroscopy (FTIR), X-ray Diffractometry (XRD), Transmission Electron Microscopy (TEM), Energy Dispersive X-ray (EDS), Raman Spectroscopy, Differential scanning calorimetry (DSC), Thermogravimetric Analysis (TGA) and Physical properties measurement system (PPMS)/Vibrating sample Magnetometer (VSM). The results confirmed the successful synthesis of uncoated and silica coated iron oxide nanoparticles with average size of 12.19±3.11nm, 14.23±2.79nm and 12.22±2.97nm for uncoated, coated1 and coated2 samples respectively with high purity single phase Fe_3O_4 inverse spinel cubic structure. The average coating thickness of coated1 and coated2 samples were found approximately 1.76±0.48nm and 1.34±0.39nm respectively. DSC and TGA, confirmed the good thermal stability of SMNP up to 900^0C and revealed that, the silica coating most probably protects the MNP core from phase transition near 590^0C. The saturation magnetization and coercivity decreased continuously with increasing temperature except the Verwey transition point which was observed at 120K in MNP, although the effect was not so prominent due to the small particle size effect, which is an important characteristic for low temperature applications. Near room temperature (300K), The particles obtained better superparamagnetic properties. The saturation magnetization of SMNP (54.5emu/g) was found lower than the MNP (62.9 emu/g) due to the coating effect but still retained the superparamagnetic properties. Smaller and Uniform particle size distributions, possibility to be further modified by functional groups (presence of Hydroxyl groups) required for specific heavy metal or radionuclides separation and excellent superparamagnetic properties support the potentiality of these synthesized SMNPs to be used in future environmental remediation and waste management applications.

1. Introduction

Continuous development of Nanotechnology and its application is playing a very significant role in almost every aspects of scientific improvement of modern world. From last few decades, numerous research and development works are being carried out on the applicability of nanomaterials in many fields from biotechnology, medical science, environmental remediation to energy industry [14].

Environmental remediation or removal of pollutants and contaminants from water, soil, rivers etc. is a very serious issue for many countries and the contamination is not only happened by the natural sources but largely coming from the human activities such as waste from agricultural, urbanization and industrial activities [54, 77]. Although few heavy metals (Fe, Zn, Cu etc.) are necessary for biological system in certain amounts, lots of Heavy metals (Pb, As, Ni, Cr, Cu, Zn, Cd, Hg etc.) are found in environmental media, irrigation and drinking water, which have very serious health effects from various acute to severe diseases (abdominal abnormalities, anemia, hypertension, Asthma, cancer, kidney failure etc.) if consumed above the safe limit [65]. Besides heavy metals, Radionuclides contaminations from both natural (^{222}Rn, ^{226}Ra, ^{228}Ra, ^{238}U, ^{232}Th etc. mainly found in ground water) and artificial radionuclides (^{131}I, ^{137}Cs, ^{99}Tc, ^{90}Sr, ^{241}Am etc.) from industrial and medical sources possess big concern for its highly hazardous environmental and health concerns [54]. Management of Nuclear Waste coming from the Nuclear power plants, Fuel processing plants, nuclear weapon production facilities and other non-power nuclear applications and nuclear medicines, is still a very challenging issue to be resolved and lots of research works are being carried out to find an appropriate solution using recent development of nanotechnology [24].

Environmental Pollution specially the water pollution is a big problem in Bangladesh, a country with rapidly developing economy. Waste water discharged from the textile, dye, paint, leather, ceramic, agrochemical industries and mixed with river and other water sources are reported as the main contributor to the water pollution in Bangladesh [59]. In their study (Ahmed, Matsumoto & Kurosawa, 2018), authors found the heavy metals Zn (13.7mg/l), Cr (o.85mg/l), Cu (6.4mg/l) and As (0.16mg/l) in the irrigation water in Gazipur district, Bangladesh are in much higher concentration than the permissible limit (2mg/l, 0.1mg/l, 0.2mg/l, 0.1mg/l respectively). High concentrations of As found in groundwater is a major health issue for millions of people in Bangladesh [78]. In some other studies (Ahmad et al. 2010; Mokaddes, Nahar & Baten, 2013; Bhuyan et al. 2019), many heavy metals such as Pb, Cd, Ni, Cu, Cr, Al, Mn, Co, Hg etc. are found with higher concentration than permissible, in sediment and surface water of some rivers (Buriganga [56], Brahmaputra[60]). Bangladesh has a research reactor and many radioactive wastes are also produced from medicine, research and industries [45] and a nuclear power plant is under construction now. Although Bangladesh Government has some long-term policy and plan for nuclear waste management [45] but finding a better solution for radionuclides remediation is always a research concern along with the world.

Magnetic nanoparticles (MNP) are already used in many applications and have great potential to be used in lot more advance application in Biomedical, Environmental and Nuclear Fields [14]. Although MNPs have shown good potentiality but still it has some limitations in aqueous and highly acidic solutions such as agglomeration, dissolution and leaching tendencies [2, 53].

Different types of surface treatment or modification techniques such as surface coatings (core-shell structure) were and are being studied to overcome the limitations of bare MNPs to make it more compatible in biological system, and adverse environments [14].

According to the many recent results, Silica coating can overcome the limitations of bare MNPs in aqueous and acidic environment and also increase the adsorption capacity in many cases [53, 66]. Recently, Silica coated MNP gained a lot of interest in many advance applications such as drug delivery [1], Nanowarming [5], DNA extraction [8], Heavy Metal removal (As [17, 55], Cu, Pb & Cd [34], Sb [31], Hg [7]), radionuclides separations (I [32], Sr [67], Cs [68]), vitrification, compaction of nuclear waste and final disposal [69] etc.

Nanotechnological approach with silica coated iron oxide nanoparticles (SMNP) could also be a good solution for remediation of the water contaminants in groundwater and rivers of Bangladesh reported above and in future radioactive waste management.

The synthesis procedures of MNPs were widely studied by different chemical, physical and biological methods. Many studies were also reported for synthesis and characterization of SMNPs. There are mainly three methods were reported for synthesis of SMNPs (Stöber [3, 4, 10], Microemulsion [11, 18] and Sonochemical [20]. Each method has some advantages, disadvantages and requires specific lab facilities. In some cases, the synthesized SMNPs were also further surface modified by different functionalization groups such as Amino [34], Thiol [7], Silane [55], imidazole [32] etc. The main source of silica used for the coating is tetraethyl orthosilicate (TEOS) which is a very expensive reagent. There is lots of variation in amount of concentration of TEOS used in previously reported synthesis procedures. The most important Property of SMNPs for its wide potential applicability is to prevent agglomeration of MNPs with retaining the superparamagnetic nature of it. With variation of TEOS concentration and other reaction conditions, these structural and magnetic properties of SMNP are varied. The performance of the SMNPs is also depends on the size of the synthesized nanoparticles.

In this work, the synthesis of Silica coated Iron oxide nanoparticles were performed using the available lab facilities choosing the optimized (TEOS concentration and other chemical substances) and simplified synthesis approach. Iron oxide were synthesized previously in the lab by most widely used and simplified chemical coprecipitation technique. Then the details chemical and structural characterizations were performed on both uncoated and coated samples using Fourier Transforms Infrared Spectroscopy (FTIR), X-ray Diffractometry (XRD), Transmission Electron microscopy (TEM), Energy Dispersive X-ray (EDS), Raman Spectroscopy, Differential scanning calorimetry (DSC) and Thermogravimetric Analysis (TGA). The detail temperature and field depended magnetic properties were measured by Physical properties measurement system (PPMS)/Vibrating Sample Magnetometer (VSM). All the properties measured, were analyzed to confirm the successful synthesis of uncoated and coated MNPs and presence of required properties needed for the applicability of these Magnetic nanoparticles for removal of environmental pollutants and contaminants in future.

2. Literature Review:

There are lots of interest in synthesis and study the structural, magnetic and other physiochemical properties of Magnetic Iron Oxide nanoparticles (MNP) and coated MNPs for their strong potential in many advance applications of modern nanotechnological advancement. In literature (Mahmudi et al, 2010 [1]; Dave & Chopda, 2014 [2]; Ali et al, 2016 [14]), synthesis, physio-chemical properties and applications of Iron Oxide nanoparticles were discussed in details. MNPs are very reactive in air/oxidizing agent and become agglomerated easily as large clusters in aqueous solution and biological system [2, 6]. It is mentioned (Dave, 2014) that, the presence of Hydroxyl groups also makes them to be surface modified by different functional groups to make them stabilized and suitable for biological and aggressive environment. With proper surface coating, the agglomeration and corrosion of MNPs can be prevented [6, 14]. Various coating materials such as gold, silver, silica, TaO_x, polymer, carbon etc. are used to protect MNPs [14]. Among these coating materials, Silica coated MNP (SMNP) is widely used [6, 7]. The main advantages of silica coating are:

a. Silica Coating makes the MNPs hydrophobic and provide high stability and biocompatibility in aqueous conditions in very wide range of pH (Lee, Fatima & Kim, 2018) [4].
b. Easy bioconjugation with different chemicals and molecules such as dye, drug and even quantum dot can be conjugated (Ali et al, 2016).
c. High heating and thermal stability with biocompatibility (Gao et al. 2020) [5].
d. Silica coating inhibits leaching of MNPs in highly acidic conditions (Han et al. 2010) [53].

2.1 Synthesis Procedures:

Synthetization of Iron oxide nanoparticles are well established and widely investigated. There are mainly three methods (Physical, Chemical and Biological) to synthesize the bare MNPs which is summarized in figure 2.

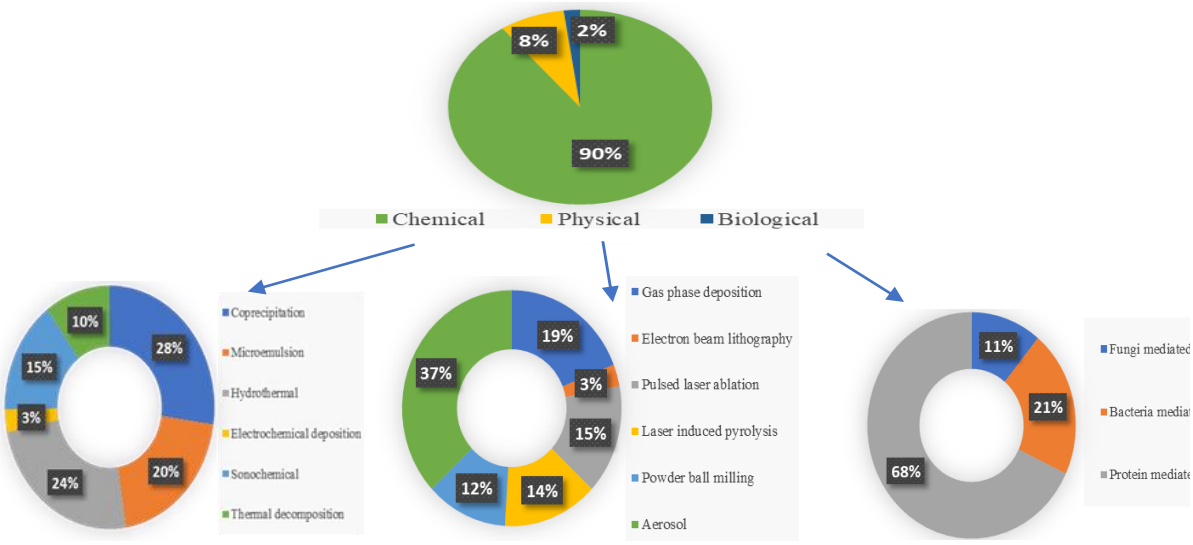

Figure 2.1: Synthesis methods of Iron Oxide Nanoparticles (data adopted from [2, 14])

The most widely used method is chemical coprecipitation due its easy synthesis process, which involves the mixture of Fe^{2+}/Fe^{3+} salt (1:2 molar ratio) in aqueous medium with a base in oxygen free atmosphere in the pH range 9-14 to have complete precipitation as the reaction written below [2, 14]:

$$Fe^{2+} + 2Fe^{3+} + 8OH^- \rightarrow Fe_3O_4 + 4H_2O$$

Silica coated Iron Oxide nanoparticles (SMNP) are mainly synthesized by following methods:

1. Stöber / modified Stöber Process [3 - 10]
2. Microemulsion / reverse microemulsion method [11, 12, 18, 22]
3. Sonochemical Approach [20, 62]

The Stöber process is named after Werner Stöber who developed the method (Stöber & Fink, 1968) for controlled growth of spherical silica particles. The authors summarized that it was done "by means of hydrolysis of alkyl silicates and subsequent condensation of silicic acid in alcoholic solutions with ammonia catalyst" [13].

During last two decades, many works on synthesis of SMNPs were done using the Stöber process with slight modification in chemical reagents (silica source), catalyst, reaction mixing time and procedure. In most of the cases, the reagents use for the silica coat is tetraethyl orthosilicate (TEOS). The hydrolysis and condensation reaction of TEOS and bond formation with MNP is shown below [43, 61]:

$$Si(OEt)_4 + 4H_2O \xrightarrow{\text{hydrolysis}} Si(OH)_4 \xrightarrow{\text{condensation}} (SiO_2)_n + n\,(H_2O)$$

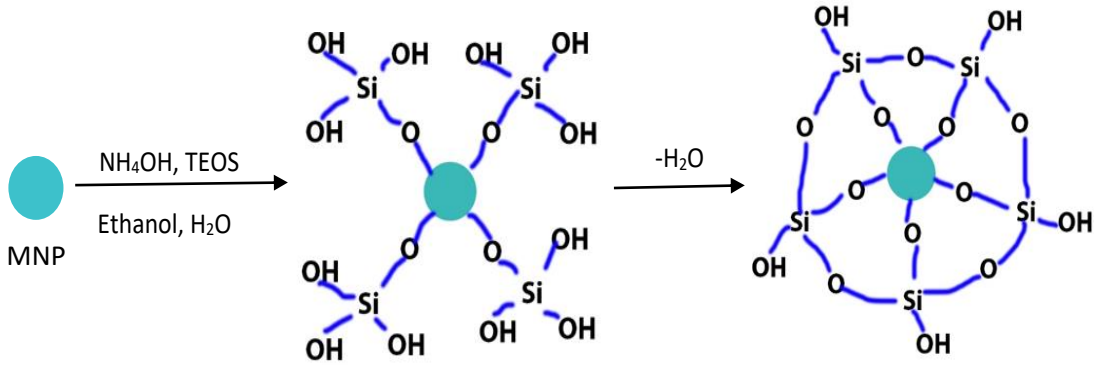

Figure 2.2: Hydrolysis and Condensation of TEOS on MNP [43, 61]

The chemical reagents, catalyst, alcoholic medium (mainly ethanol), distilled water (DI) and their concentrations used in some of previous researches for coating different amount of MNPs are summarized in Table 2.

Table 2.1: Materials used in SMNP synthesis (Previous Methods)

Bare MNP(g)	Ethanol (ml)	DI (ml)	Catalyst (ml)	TEOS (ml)	References
0.045	80	16	2 (25wt% NH_4OH)	0.8	[21]
0.1	80	20	1 (28wt% NH_4OH)	0.1	[17]
0.1	80	20	1 (28wt% NH_4OH)	1-7 (in 47ml ethanol)	[4]
0.1	80	20	1 (2M NaOH)	0.1	[16]
0.5	50	5	5 (10wt% NaOH)	0.2	[10]
0.5	80	20	2 (25% NH_4OH)	0.2	[27]
2.0	160	40	5 (25% NH_4OH)	1-7	[19]

The effect of type of alcohol, alcohol/water ratio, amount of catalyst and TEOS on the synthesis of SMNP with 2g of bare MNP were investigated by Deng, Wang, Hu, Yang & Fu (2005). In this study (Deng et al, 2005), methanol, ethanol, isopropanol and n-propanol were used as alcoholic medium and ethanol was found as the best alcohol type to get uniform SMNPs. Deng (2005), also varied ethanol/water ratio from 1 to 5 and concluded that, ethanol/water ratio at 4 is the best option to get SMNPs with better morphological (regular shape) and dispersion properties. They varied the ammonia solution from 1 to 9 ml keeping ethanol/water ratio at 4 with 1ml of TEOS. The data in Table 2 shows that, most of the researcher followed these findings to keep the ethanol/water ratio at 4. Authors (Deng et al, 2005) found, SMNP can formed for good range of ammonia solution concentration (1-5ml) and explained that, for higher concentration of ammonia solution (> 7ml for 1ml TEOS) can lead to formation of core free small silica particles due to rapid hydrolysis of TEOS [19]. Effect of TEOS concentration was also studied (Deng et al, 2005; Lee et al, 2018) and summarized that thickness of silica coating increases with increasing concentration of TEOS, although higher TEOS can also lead to form core free silica particles besides SMNPs. Some articles (Ahangaran, Hassanzadeh & Nouri, 2013 & Lee et al. 2018) also suggested to pretreat the bare MNPs with HCL solution prior coating process to avoid the possibility to form blank silica microspheres [4, 27]. Another study (Sharafi, Bakhshi, Javidi & Adrangi, 2018) suggested that, by decreasing the initial concentration of catalyst and increasing later gradually, may prevent MNP particles agglomeration without any pretreatment or surface modification [16].

Some of the researches also used microemulsion/reverse microemulsion to produce SMNPs. Antonio Cid (2018) described, microemulsion is a thermodynamically stable and isotropic mixture of two immiscible liquid (Oil, Water) with surfactant. It is summarized in the chapter (Cid, 2018), Controlling the reaction condition time, temperature, surfactant type, it is possible to control the

size, shape, crystal structure and production of different geometries by this method [23]. Ali et al (2016) mentioned, that removal of residual surfactants and difficulty in scale-up production is the main limitations of this methods [14].

Sonochemical approach to synthesis the SMNPs was explored by Morel et al (2008) and reported that, using powerful ultrasound for main reaction of the synthesis process, can overcome the main problems (slower process, agglomeration) of earlier Stöber Process using conventional magnetic/mechanical stirring for reaction mixing. Morel (2008) used 0.35mmol Fe_3O_4, 30ml ethanol, 0.7ml concentrated ammonia in 9.3ml water and 1.8mmol TEOS (99%) for the synthesis and described the detail procedure in his article. Morel reported that, ultrasonication can cause 5times faster hydrolysis of TEOS than conventional which decrease the reaction time significantly, prevent agglomeration and produce uniform single core SMNPs [20].

2.2 Properties, Analytical tools and Previous Results:

To confirm the successful production of MNPs and SMNPs and to explore the possibility of these particles to use in different applications, it is necessary to characterize and measure the required properties of these nanoparticles. There are lots of characterization tools are available to analyze and measure the structural, magnetic and other physiochemical properties. Some of the most important Properties and analytical methods used by the researchers in this field and their findings are briefly described below.

2.2.1 Chemical properties:

To identify the materials and functional groups present in the synthesized particles, widely used tool is Fourier Transforms Infrared Spectroscopy (FTIR), because of its easy and simple measurement technique. In this analysis, Infrared radiation (IR) is applied by the machine to analyze the chemical properties through radiation absorption and transmission of specific frequency by the sample. For the conventional FTIR technique, the powder samples need to be mixed with a salt (usually KBr) to make it translucent to the IR radiation. But, with ATR (Attenuated Total Reflectance) tool, there is no sample preparation needed because of using reflectance technique instead of transmission [61].

The main absorption bands of MNPs and SMNPs reported by the some of the previous researches are summarized in Table 2.2.

Table 2.2: IR absorption bands, cm^{-1} (Previous Results)

Tools	Fe-O stretching vibration		Si-O-Si, Si-OH, Si-O stretching and bending vibrations	Reference
	MNP	SMNP		
FTIR	580	580	1119, 963, 796	[4]

Tools	Fe-O stretching vibration		Si-O-Si, Si-OH, Si-O stretching and bending vibrations	Reference
	MNP	SMNP		
FTIR	441, 585, 632	-	1095,945,802	[35]
FTIR	572		1086, 949	[9]
FTIR	582	574	1080, 798	[43]
FTIR	584	574	1080	[17]
ATR	544, 399		1050,112	[38]
ATR	523, 311	553	1055,789	[40]
ATR	548	-	-	[37]

According to the previous results listed in Table2.2, The characteristic bonds of Silica shell (Si-O-Si/Si-OH/Si-O) in SMNP were identified in the region 800-1200 cm^{-1}. The main silica characteristic peak (Si-O-Si stretching) was found near 1080 (FTIR) or 1055 (ATR), main Fe-O vibrational bond of Fe_3O_4 was near 580 cm^{-1} (FTIR) 0r 545 cm^{-1} (ATR). The results are little bit deviated between conventional FTIR (with KBr pellet) and ATR (no additional sample preparation). The Fe-O bond position in SMNP can be shifted little bit due to formation of Fe-O-Si bond [9]. The hydroxyl groups (-OH) were also reported in FTIR analysis in both MNP and SMNP near 1614cm^{-1} and 3000cm^{-1} region [9, 15, 38]. The presence of hydroxyl groups is important for further functionalization related to different applications [2].

2.2.2 Structural Properties:

The structural properties of the nanoparticles are mainly characterized by X-Ray Diffractometry (XRD) and Transmission Electron Microscopy (TEM).
In XRD, the structural properties such as crystallinity, crystallite size, Phase Purity, Lattice constants etc. are measured from the angle and intensity of the diffracted beam by the crystallographic planes in response to the incident X-ray beams on the sample. The peaks in different diffraction angle, can characterize the specific crystal plane in crystalline samples. The brag angles, d_{hkl} (distance between two parallel planes) and corresponding planes of different Iron oxide phases in the magnetite rich powder reported in the study (Noval & Carrazo, 2019) is adopted in Table 2.3.

Table 2.3: d_{hkl} and Planes of different Iron oxide Phases in Magnetite rich Powder (Noval & Carrazo, 2019) [12]:

angle, $2\theta^0$	d_{hkl}, Å	Miller indices (hkl)	Phase
18.4	4.81	(111)	Fe_3O_4

angle, $2\theta^0$	$d_{hkl,}$ Å	Miller indices (hkl)	Phase
24.2	3.67	(012)	α-Fe_2O_3
30.1	2.96	(220)	Fe_3O_4
33.2	2.70	(104)	α-Fe_2O_3
35.5	2.52	(311)	Fe_3O_4
37.2	2.41	(222)	Fe_3O_4
41.8	2.16	(200)	FeO
43.2	2.09	(400)	Fe_3O_4
49.6	1.84	(024)	α-Fe_2O_3
53.5	1.71	(422)	Fe_3O_4
54.1	1.69	(116)	α-Fe_2O_3
57.0	1.61	(511)	Fe_3O_4
60.6	1.52	(220)	FeO
62.6	1.48	(440) (214)	Fe3O4 α-Fe_2O_3
74	1.28	(533)	Fe_3O_4

For pure single-phase magnetite (Fe_3O_4), Most of the previous results reported the corresponding planes and angles are, 2θ = 30.1, 35.5, 43.2, 53.5, 57, 62.6 & 74 for plane (220), (311), (400), (422), (511), (440) & (533) respectively [4, 17, 27, 42, 44].

In TEM, the surface morphology, particle size measurement and distribution can be measured directly at much higher resolution than other microscopy techniques by using electron beam. In HRTEM (High Resolution TEM), study of materials properties can be done at atomic scale. With EDS (Energy Dispersive X-ray spectroscopy) attachment of TEM, the elemental analysis and compositional mapping can be done [63].

Comparative particle size, crystallite size of MNPs and SMNPs synthesized by different methods and reported by previous researches are summarized in Table 2.4.

Table 2.4: Particle size, crystallite size of MNPs and SMNPs synthesized by different methods (Previous Results)

Synthesis method 0f SMNP	Particle size, nm (TEM)		Crystallite size, nm (XRD)		Reference
	MNP	SMNP	MNP	SMNP	
Modified Stöber	14.29±4.05	15.41±4.11	12.7	-	[44]
Modified Stöber	8-16	16-24	12	20 (agglomeration	[10]

Synthesis method 0f SMNP	Particle size, nm (TEM)		Crystallite size, nm (XRD)		Reference
	MNP	SMNP	MNP	SMNP	
				inside nanosphere)	
Modified Stöber	9	53 (5 aggregate)	-	-	[3]
Modified Stöber	-	-	46.7	26.3	[41]
microemulsion	24 (mean)	35.3±0.04	9.44±0.02	16±0.14 (large amount of silica, resulted in expansion micelles)	[11]
Reverse microemulsion	20.6±-1	30.2±1.7	-	-	[18]
coprecipitation	13.4	16.6	12.09	13.02	[34]
coprecipitation	100 (agg)	30-100	-	-	[6]
sonochemical	4-10	10 (core) + shell 3.5 (3h)/ 1.1 (1h)	-	-	[20]
sonochemical	6-15	6nm silica shell	10	-	[9]

From Table2.4, it is confirmed that MNPs has large tendency to aggregate in many cases. For most of the applications, large aggregate need to be avoided. Smaller particles have more surface area, superparamagnetic properties and uniform distribution for better applicability. with optimization of reagent and catalyst concentration, ethanol/water ratio and controlling hydrolysis rate of TEOS, it is possible to produce better SMNPs [19, 20].

Another analytical tool, Raman spectroscopy is used to determine the formation of vibrational modes present in MNPs and SMNPs to confirm chemical bonds and phases present in the samples [49, 64]. Majumder et al. (2015) [41], reported the characteristics bonds of Fe-O stretching at 678 cm^{-1} and Vibrational modes related to Fe_3O_4 at 545 cm^{-1} and 300 cm^{-1}. Similar stretching and vibrational bonds of Fe-O related to Fe_3O_4 were reported at 596, 489 and 396 (Yew et al. 2017 [63]), at 670, 538,306 (Yuvakkumar and Hong, 2014 [64]). Majumder et al. (2015) also reported the peaks at 480, 365 and 216 cm^{-1} are characteristic bond of silica and mentioned that presence of silica bonds with decreased intensity and slight positional shift of Fe-O bonds confirms the silica coating on Fe_3O_4.

2.2.3 Magnetic Properties:

The magnetic properties of Iron nanoparticles gained great interest for its superparamagnetic behavior or very low remanence and coercivity with greater surface area. These properties make them very suitable candidate for many applications in biomedical, environmental and nuclear field [14].

The magnetic properties are mainly investigated by Vibrating sample Magnetometer (VSM) or Physical properties measurement system (PPMS). VSM can measure the magnetic moment as a function of applied Magnetic field at different temperatures. Under an external magnetic field applied, magnetic moment is increasing until it reaches a saturation value termed as Saturation Magnetization (Ms) and the value of magnetic field where the magnetic moment is zero is termed as coercivity/coercive field (Hc).

Magnetic properties depend on various conditions such as particle shape, size, spin canting, crystal defects, temperatures etc. (Hu et al. 2018) [72]. Li et al. (2017) explored the size effect on magnetic nanoparticles in terms of critical size to change from single domain to multidomain structure and they found 76nm is the critical size for magnetite nanoparticles [71].

Temperature dependent Saturation magnetization (Ms) and Coercivity (Hc) is expressed by Kneller's Law and Bloch's Law (Nayek et al. 2017) [70] as follows:

$$M_S\,(T) = M_0\left[1 - \left(\frac{T}{T_o}\right)^{\alpha_B}\right]$$

$$H_c(T) = H_o\left[1 - \left(\frac{T}{T_B}\right)^{\alpha_K}\right]$$

Where,

M_0 = Magnetic Moment at 0K

T_0 = Temperature at Zero Magnetic Moment

T_b = superparamagnetic blocking temperature below where the single domain, uniaxial anisotropy is present [70]

α_β and α_k is the Bloch's and Kneller's exponent respectively with well-known values of 0.5 and 1.5 for bulk materials.[70].

In their study (Nayek et al. 2017), authors explored that the Kneller's and Bloch's exponents values were changed with decreasing the particle size and mentioned that finite size effects or large anisotropy in nanoparticles, inter-particle interactions and spin-glass structure formation could be the reasons [70].

Another important phenomenon for low temperature applications of Magnetite nanoparticles is Verwey transition (Tv), where sharp transition in magnetic properties is happened at 120K-130K region [72, 74]. Although the authors (Bohra, Agarwal & Singh, 2108) mentioned that the Verwey transition is weakly size dependent but suppressed below 20nm particle size and completely disappear below 6nm [74].

The temperature and size dependent Magnetic properties of Magnetite (Fe_3O_4) nanoparticles are summarized in Table 2.5 from the data of previous results reported.

Table 2.5 Magnetic Properties of Magnetite nanoparticles (Previous Results)

Temperature (K)	Particle size (nm)	M_s (emu/g)		Hc (Oe)		References
		MNP	SMNP	MNP		
2	12	78	-	250		[70]
50		77		80		
100		77.5		40		
200		74		39		
300		70		38		
5	2-20	84.6	-	584.7		[72]
128		86.2		280.3		
300		79.7		338.1		
300	-	86	62	95	153	[40]
	10	68	36.2	80	60	[20]
	200-300 (agglomerated)	85	67	low (hysteresis loop)		[4]
	100	44.8	30.2			[6]
	6-15	79	46.99			[9]
	8-16	64.8	40.3			[10]
	100	78	58			[17]
	13.4	68	36.2			[34]
	9.6	54.7	-	Near Zero		[71]
	287	84.7		190		

From table2, it is seen that, with increasing temperature the saturation magnetization and coercivity is decreased except near 128K which can be attributed to the Verwey transition mentioned above. The Ms and Hc values for all the reported cases in Table2.5, indicate the superparamagnetic behavior of Fe3O4 near room temperature. Although, the Ms values for the SMNP is lower than the bare MNPs because of the coating effect, still it has enough magnetic properties to retained the

superparamagnetic nature of bare magnetite [40]. The extend of decrease in magnetization values in coated sample depends on the thickness of silica coating, as the coating thickness increases, the magnetization decreases [19].

2.2.4 Thermal properties:

The thermal properties are measured by Differential Scanning Calorimetry (DSC) and Thermogravimetric Analysis (TGA) techniques. DSC measures the heat flow and TGA measures the sample mass changes against temperature and/or time changes. These experiments provide information regarding thermal stability, weight loss (decomposition of chemical compound or evaporation of volatile elements etc.), weight gain (oxidation, adsorption etc.), phase transition, decomposition kinetics etc. over the tested temperature ranges [66].

According to the previous reported results (Du, Liu, chu & Zhang, 2005 [43]; Sneha, Nachiappan, Sundaram, 2015 [25]) both MNPs and SMNPs show good thermal stability. In their studies, (Du et al. 2005) and Sneha et al. 2015), the initial endothermic peak around 100-300^{0}C was reported as removal of physical/chemical water and decomposition of alcohol or any residual chemical substances. In their studies (Sneha, 2015 and Aghazadeh, Karimzadeh & Ganjal, 2019 [29]) a small endothermic peak in DSC curve with little weight loss near 550-600C was reported as probable crystallization of magnetite phase or phase transition of Fe_3O_4 to FeO.

2.2.5 Adsorption properties:

MNPs and SMNPs with proper surface functionalization, exhibit very good adsorption properties for removal of heavy metals and radionuclides from aqueous solution [2, 6, 7, 17, 31, 32, 34, 54, 55]. The required amount of adsorbent (SMNP) is dispersed in the solution containing the elements (natural or stock solution prepared) and adsorption reaction is performed for certain times. Then the adsorbent is separated magnetically from the solution. The adsorption capacity is mainly measured from the concentration of the element to be adsorbed in the solution before and after the adsorption reaction with SMNPs as following simple formula [6, 17]:

$$Q_{ad} = \frac{C_0 - C_t}{W}$$

$$\%C = \frac{C_0 - C_t}{C_0} \times 100$$

Where,

Qad (mg/g) = adsorption capacity (weight of adsorbed element per gram of adsorbent)

C_0 (mg/l) = initial concentration of element in the solution

C_t (mg/l) = concentration of residual element in the solution (mg/l) at time t of adsorption reaction

W (g/l) = amount of dry mass of adsorbent (SMNP) used per solution volume.

The concentrations are mainly measured by Atomic Absorption Spectrometry (AAS) [7, 31] or UV spectrophotometer [6, 32]. The maximum adsorption capacity can be determined from adsorption isotherm models. The general form of Langmuir model (L. Langmuir, 1918) and Freundlich model (Carr, Freundlich and Sollner, 1941) are as follows (as cited in Madrakian et al. 2012) [32]:

Langmuir model,

$$\frac{a_L q_e}{K_L} = \frac{K_2\, C_e}{1 + K_2 C_e}$$

Freundlich model,

$$q_e = K_F C_e^{\frac{1}{2}}$$

Where,

Ce (mg/l) = equilibrium concentration of the element in the solution (mg/l in Langmuir, mmol/l in Freundlich model)

q_e (mg/g) = adsorption capacity (weight of adsorbed element per gram of adsorbent)

a_L (l/mg) and K_L (l/g) are the Langmuir constants with a_L related to the adsorption energy

Kf ($mmol^{1-1/n}\ L^{1/n}$ /g) and 1/n (n related to adsorption energy distribution) are Freundlich constants Maximum adsorption capacity, q_m (mg/g) = K_L/ a_L [32].

The detection and adsorption capacity of SMNP are presented in Table 2.7.

2.3 Applications of SMNPs:

2.3.1 Biomedical Applications:

Some of the important biomedical application of silica coated Iron oxide nanoparticles are summarized in Table 2.6.

Table 2.6: Biomedical Applications of SMNPs

Applications	Scope	Particles and advantages	References
Diagnostic	MRI contrast Agent for Magnetic Resonance Imaging (MRI) (cancer diagnosis, stem cell tracking, gene expression etc)	Surface modified SMNP (negligible side effect, Biocompatible)	[1, 26]

Applications	Scope	Particles and advantages	References
Therapeutic	targeted drug delivery (anti-arthritic, anti-inflammatory, hyperthermia, radioactive, chemotherapeutic etc.)		
Nanowarming	promising solution to rewarm organ rapidly and uniformly which is very important for cryopreservation (long term banking of biological system)	SMNP (High heating, stable and easy wash out)	[5]
Detection of Pathogenic Viruses	PCR based detection	SMNP (Faster, Higher Sensitivity)	[15]
DNA extraction	Extraction, Purification	Amino functionalized SMNP (high acid resistance, better adsorption and purity)	[8]

From Table 2.6, it is seen that the biocompatibility, high aqueous and thermal stability, easy separation, higher sensitivity and easy conjugation with application specific functional groups make the SMNPs ideal choices for diverse biomedical applications.

2.3.2 Environmental Applications

SMNP can be used for both detection and removal of toxic elements from aqueous environment. The adsorption capacity of SMNP for different elements and sources, reported in some of the previous articles are summarized in Table 2.7.

Table 2.7: Adsorption capacity of SMNP for Metal and Radionuclides (Previous Results):

Element	Source	Detection limit (ng/ml)	Adsorbent	Adsorption capacity	Reference
As(III)	stock solution	-	SMNP	67.92 µg/g	[17]
As(V)	Sodium Arsenate heptahydrate	-	MNP Silane modified SMNP	157 µmol/g 170 µmol/g	[55]
Cu(II) Ni(II) Co(II) Cd(II)	Stock solution	4.7 9.1 9.5 2.3	Modified SMNP	-	[66]

Element	Source	Detection limit (ng/ml)	Adsorbent	Adsorption capacity	Reference
Pb(II) Mn(II)		7.4 15.3			
Hg	Rain water	1.41±0.17	Thiol modified SMNP	101 mg/g	[7]
	Well waters	0.34±0.02			
	Sewage water	1.3±0.17			
Humic Acid	water	-	MNP SMNP	95.15 196.07 mg/g	[6]
Cu(II) Pb(II) Cd(II)	Stock solution	-	Amino functionalized SMNP	0.47 mmol/g 0.37 mmol/g 0.20 mmol/g	[34]
Sb(III)	Strong acid solution (2.5M H_2SO_4)	-	Amino functionalized SMNP	45.3mg/g	[31]
I	Stock solution	-	Imidazole modified SMNP	140.84 mg/g	[32]
Sr(II)	$SrCl_2$ solution	-	Titanium modified SMNP (Fe3O4@SiO2@TiO2)	37.1 mg/g	[67]
Cs-137	Contaminated sea water	-	Ptassium Titanium Ferrocyanide SMNP (Fe3O4@SiO2@KTiFC)	43.09 mg/g	[68]

It is seen in Table-2.7 that, Silica coated Magnetite with surface modified by target specific functional groups/chelators are preferred over bare magnetite and shows higher adsorption capacities.

2.3.3 Nuclear Waste Management:

Removal of radionuclides from contaminated solution and nuclear waste is a challenging task due to its highly acidic and hazardous environment. Magnetic nanoparticles (MNP) shows great potentiality for removal for radionuclides from contaminated solution by adsorption and magnetic separation technique as the steps summarized below (D. Nath, 2018) [24].

1. Synthesis of MNPs with higher Magnetic Susceptibly and surface area
2. Surface coating and functionalization for higher stability in highly acidic environment and adsorption capacity
3. Conjugation with Chelators/functional groups for specific radionuclides/actinides
4. Radionuclides/actinides extraction reaction

5. Separation and stripping of Radionuclides
6. Recycling of MNPs and Actinides or waste disposal

Agglomeration, Dissolution and leaching of bare MNPs in acidic solutions and external environmental conditions limit their applicability. Silica coat can protect MNPs from these limitations and make it suitable for applications in aggressive environment (Han et al. 2010 [51], Yi et al. 2014 [68].

Silica coated MNPs (SMNP) conjugated with proper functional groups (shown in table-2.7) has shown good separation and adsorption efficiency for many radionuclides/actinides from stock solutions, contaminated water, seawater sources [32, 51, 53, 54, 68].

Litvinenko, Zabulonov, Kadoshnikov & Yurzhenko, 2012 [69], also explored the possibility of Fe_3O_4/SiO_2 nanocomposite for vitrification, compaction and disposal of nuclear waste. According to their study (Litvinenko et al. 2012), Fe_3O_4/SiO_2 forms glass phase at 1000^0C which produce the solid matrix for retention of incorporated radionuclides by it and this can be useful for vitrification, compaction and further waste disposal.

3. Objectives of the Present Work:

The main objective of this internship/thesis work is to synthesize the silica coated magnetite nanoparticles to be used in future applications for environmental remediation (separation of toxic heavy metal/radionuclides), keeping in mind the alarming water pollution by heavy metals from Bangladesh perspectives. The following tasks are associated with the main work:

1. To synthesize silica coated Magnetite nanoparticles by most widely used Stöber method taking into account the recent improvements and less frequently used sonochemical approach claimed better performance in terms of agglomeration tendency of magnetite nanoparticles with faster synthesis process.

2. To characterize the synthesized uncoated and silica coated magnetite nanoparticles in details to confirm their successful synthesis and obtain the information on chemical bonding, crystallographic information, surface morphology, dimensions, thermal stability and magnetic properties. In addition, To measure detail temperature dependent magnetic properties of magnetite nanoparticles to observe some interesting low temperature phenomena reported in literatures.

3. To analyze all the properties measured to comment qualitatively on the feasibility of these synthesized nanoparticles to be used in future applications for removal of heavy metal/radionuclides from aqueous solution by adsorption process.

4. Experimental Methods and Setup:

4.1 Materials and Synthesis

Silica Coated Iron Oxide nanoparticles (SMNP) were synthesized via modified Stöber and sonochemical approach reported in many earlier researches [4, 9, 19, 20] with slight modifications and using the available laboratory facilities. Uncoated Iron Oxide Nanoparticles (MNP) were previously synthesized by chemical coprecipitation Method from mixing of $FeCl_3$ and $FeSO_4$ solution at 2:1 ratio on a hot plate (25^0C at 300rpm) under N_2 atmosphere with NH_4OH catalyst. The reaction was completed at pH 11.

Then, the silica coating was performed on these nanoparticles and detail characterizations were performed on both uncoated and silica coated MNPs.

Two Coated MNPs (Coated1 and Coated2) were prepared by two modified processes shown in table 4.1. Reaction Mixing was done by Ultrasonic Probe Sonicator for Coated2 instead of Magnetic stirrer used in Coated1. MNPs were treated in HCL before performing Coated1 process but not for Coated2 less amount of chemical substances was used for Coated2, although keeping same volume ratio of Ethanol/water and NH_4OH/TEOS.

Table 4.1: chemicals used for synthesis of coated nanoparticles

Sample	weight of MNP	Pretreatment in HCL	Ethanol	DI	NH4OH (28%)	TEOS (≥98%, Sigma Aldrich)	Methods
Coated1	1g	Yes	120ml	30ml	5ml	6ml in 44ml ethanol	Modified Stöber
Coated2	1g	No	60ml	15ml	1.4ml	2ml	Sonochemical

The TEOS concentration were kept as low as possible for the following reasons:

1. To avoid/minimize the formation of blank silica microspheres.
2. To not compromise much with the superparamagnetic properties of magnetite core.
3. To ensure optimize use of expensive TEOS reagent.

Synthesis process of SMNPs is described step by step below:

1. Coated1 Sample:

    a) 1g of MNP was treated in 50ml 1M HCL by Ultrasonic Probe Sonicator (heilscher UP400St) for 5minutes. 50ml 1M HCL solution was prepared from standard 37% HCL solution (4.15ml 37% HCL + 45.85ml Distilled Water (DI)).

b) Treated MNPs were separated from HCL and washed thrice with DI.
c) MNPs were homogenously dispersed in mixture of 120ml ethanol and 30ml DI.
d) 5ml of 28% NH_4OH was added to the mixture slowly.
e) The mixture (MNP + Ethanol + DI + Ammonia) was place on Digital Hotplate Stirrer (LabTech LMS-2003D) and heated to 40^0C.
f) 6ml of 98% TEOS (in 44ml ethanol) was added dropwise to the mixture while continuing stirring by magnetic stirrer.
g) The magnetic stirring was continued at 300rpm and 40^0C for 4.5hrs.
h) The synthesized particles were separated from the mixture by ultrasonic centrifuge separator (Hitachi CP 80NX) and washed several times with ethanol and DI.
i) The separated particles were dried in oven at 70^0C for 12hrs and kept in airtight container for characterization.

2. Coated2 Sample:

a) 1g of MNPs were homogenously dispersed in 60ml ethanol and 15ml DI and sonicated for 30minute by ultrasonic probe Sonicator at 30W.
b) 1.4ml of 28% NH_4OH was added slowly to the mixture and the sonication was continued.
c) 2ml of 98% TEOS was added dropwise to the mixture while continuing sonication.
d) The Sonication was continued for 2.5hrs and the solution was kept overnight for complete condensation.
e) The synthesized particles were separated from the mixture by ultrasonic centrifuge separator (Hitachi CP 80NX) and washed several times with ethanol and DI.
f) The separated particles were dried in oven at 70^0C for 12hrs and kept in airtight container.

Figure 4.1 shows some of the samples and apparatus used in this work for synthesis process (a. Magnetic hot plate stirrer, b. Ultrasonic Probe Sonicator, c. UltraCentrifuge, d. Synthesized Samples kept in Ethanol, e. Magnetic separation, f&g. Dried Sample).

(a) (b) (c)

(d)

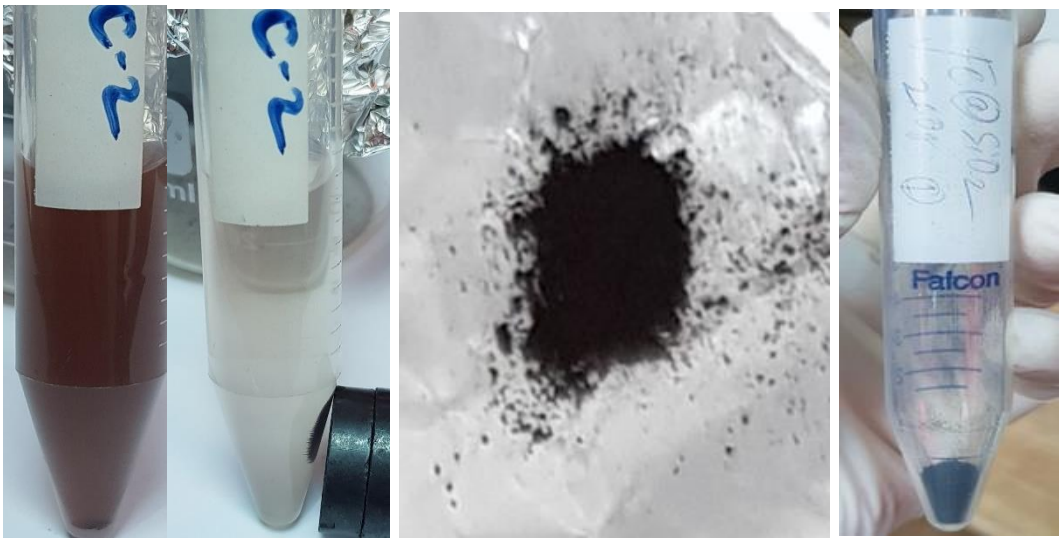

(e) (f) (g)

Figure 4.1: Apparatus used for synthesization process and separation of synthsized samples

4.2 Sampling and characterization:

Sample preparation for different charcaterization techniques and characterization tools used in this work, are briefly described below:

4.2.1 Fourier Transforms Infrared Spectroscopy (FTIR):

For, FTIR analysis, generally the powedered samples were prepared as pellet mixing with KBr. In this work, the ATR attachment (UATR Two) of the Machine 'Spectrum Two FTIR Spectrometer – PerkinElmer' was used to measure the FTIR spectrum directly on the dried powdered samples.

This machine has a diamond crystal with a pressure arm to ensure the good contact of the sample with diamond crystal. The diamond crystal was cleaned with alcohol before each measurement to avoid any previous contamination. After correcting background response and adjusting the force gauge, ATR spectra of each sample were collected in the wavelength range 350cm^{-1}- 4000cm^{-1} with accumulation of 100scans.

4.2.2 X-ray Diffractometry (XRD):

The powder samples were placed on the XRD sample holder uniformly and put in the XRD machine (Rigaku SmartLab). The incident X-ray wavelength was 1.54Å and the spectrum was collected in the angle range 10-80^0 with 0.02^0 step width. Crystallinity, crystallite size, interplanar spacing, Phase Purity, Lattice constants etc. are determined by analyzing the XRD data. The crystallite size, interplanar spacing or distance between two parallel planes and lattice constant were measured using the following Debye-Scherrer formula [44].

Crystallite size,

$$D = \frac{K\lambda}{\beta cos\theta}$$

Interplanar spacing,

$$d_{hkl} = \frac{\lambda}{2sin\theta}$$

Lattice constant,

$$a = d_{hkl}\,(h^2+k^2+l^2)^{0.5}$$

Where, k = shape factor = 0.9

λ = incident x-ray wavelength (Å)

β = Full Width Half Maximum (radian)

θ = Brag Angle (radian)

h, k , l = miller indices of plane

4.2.3 Transmission Electron Microscopy (TEM):

The bright field image, dark field image, EDS (Energy dispersive x-ray spectroscopy) spectrum and Mapping were taken by TEM (Talos TEM, ThermoScientific) to analyze the particle size and distributions, crystallographic information and elemental analysis of uncoated and coated samples. Small amount of the dried powder samples was sonicated in ethanol for 15 minutes by ultrasonic probe Sonicator to form solution. Then very small amount of the solution was put on the copper grid, dried and inserted to TEM for analysis. The particle sizes, crystalite size and d_{hkl} were measured manually by image processing software (Digimizer) on the images taken by TEM.

4.2.4 Raman Spectroscopy:

For Raman analysis were done with the The MonoVista CRS+ (S&I) Raman Microscope. the powdered sample were pressed with KBr salt to form pellet to analyze and the light source used was 785nm Laser beam.

4.2.5 Differential Scanning Calorimetry (DSC) and Thermogravimetric Analysis (TGA):

DSC and TGA analysis were performed by putting the nanoparticles in the sample crucible of the DSC instrument (NETZSCH STA 449 F3). The test temperature range were set from 28^0C to 1020^oC at 40^0/min rate. The differential weight loss curve was plotted to observe any sharp changes in mass of the sample.

4.2.6: Magnetic Properties Measurement:

The detail magnetic properties of MNPs were measured by Physical properties measurement system (Dynacool PPMS by Quantum Design). 10 mg of uncoated and 5mg of coated sample were used for all the test measured by PPMS system and normalized the values for per gram of sample. The magnetic properties of uncoated sample were measured at temperature range 5K-920K and applied field range ±20Oe upto ±5T. The coercivity (field needed to reverse the magnetization or field at zero magnetic moment) for each temperature and field is measured from the extrapolation of the data obtained from hysteresis loop of each temperature and field.

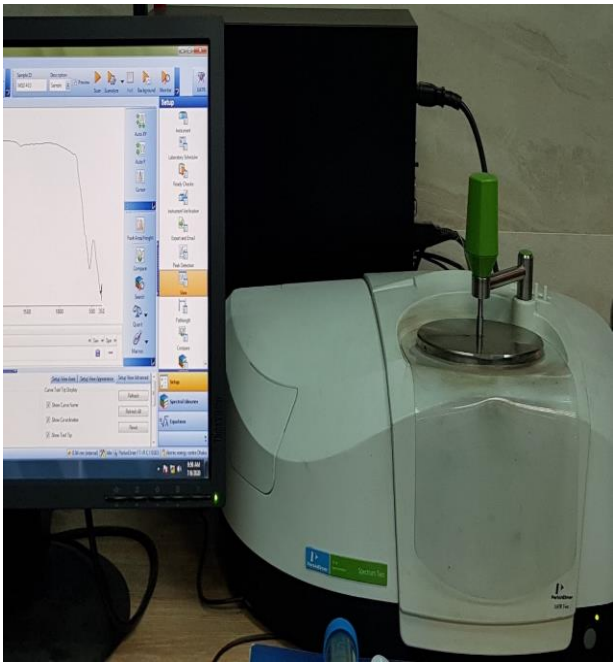

FTIR

XRD

TEM PPMS/VSM

Figure 4.2: Some of the characterization and measurement tools used

5. Results and Discussion

5.1 FTIR Spectra:

The ATR/FTIR spectra from wavelength 350 to 4000 cm^{-1} of uncoated/bare Magnetite nanoparticles (MNP) and silica (SiO_2) coated MNP (SMNP) is presented in figure 5.1.

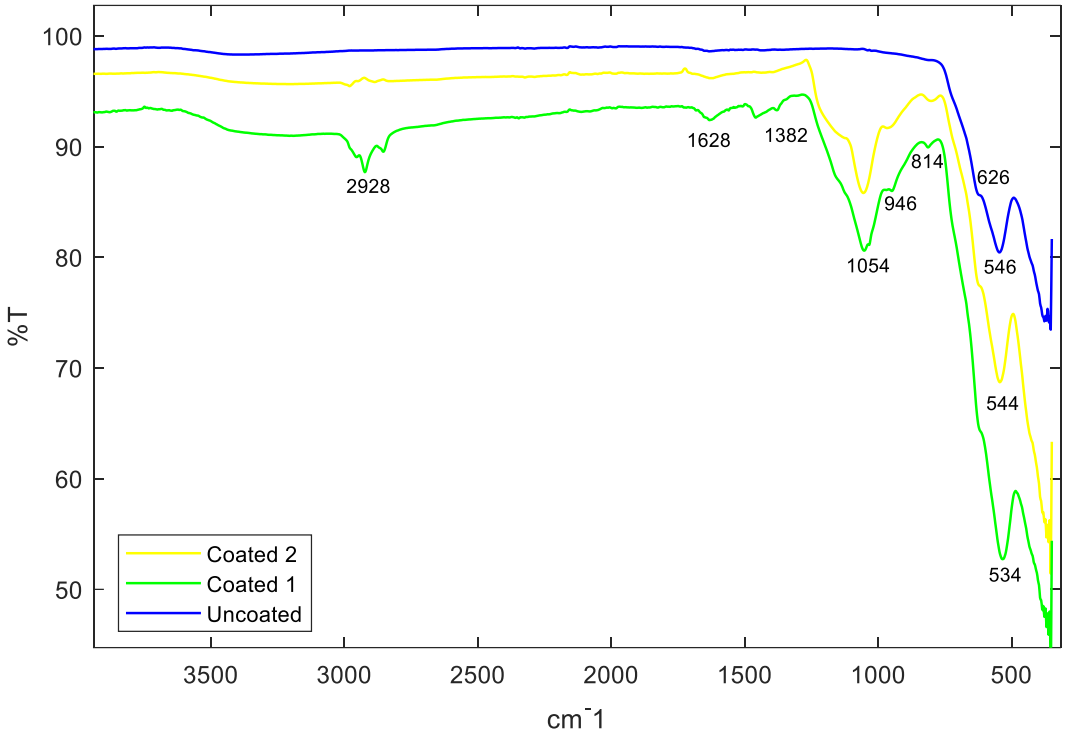

Figure 5.1: ATR spectra of Uncoated and Silica Coated MNP

The sharp band at 546 cm^{-1} following a small shoulder near 626 cm^{-1} represent the Fe-O stretching vibrational band [37, 38, 41] in bare MNP. Although in some articles, the Fe-O stretching vibration was reported around 572-588 cm^{-1} [9,10,17,35], Lesiak et al., 2019 mentioned that those measurements were done on MNP pellet formed with KBr, which may shift the peak position [37]. Bands near 1382 cm^{-1} and 1628 cm^{-1} corresponds to Fe-O groups vibration [42] and O-H stretching [35,38]. Peaks around 3000 cm^{-1} represents hydroxyl groups [15, 38]. The introduced silica network (different silica functional groups) in SMNPs is revealed between 800 to 1100 cm^{-1} region in both coated 1 and coated 2 spectra. The strong band near 1054 cm^{-1} corresponds to Si-O-Si stretching vibration mode [38, 40], weak bands near 946 cm^{-1} and 814 cm^{-1} are for Si-OH stretching and Si-O bending [4, 17, 35]. Besides, the Si-O stretching and bending vibration, some literatures [15, 40, 50, 51] also reported, Si-O-Fe bond formation in this region (945-1250 cm^{-1}) for SMNP. The Fe-O bond, slightly shifted in coated 1 (534 cm^{-1}) and in coated 2 (544 cm^{-1}) indicates the presence of Fe-O-Si bonds [41-43] in the SMNP. The above results (Fe-O bonds, formation of silica matrix and Si-O-Fe bond) confirm the successful synthesis of bare MNPs and Silica Coated MNPs. Silica coating with presence of increasing hydroxyl groups will facilitate the easy conjugation with other target specific functional groups for different applications.

5.2 XRD Patterns:

The XRD pattern of uncoated and coated MNP are presented in Figure 5.2 and the characteristic reference peak and experimentally obtained peak values of MNP are shown in Table 5.1.

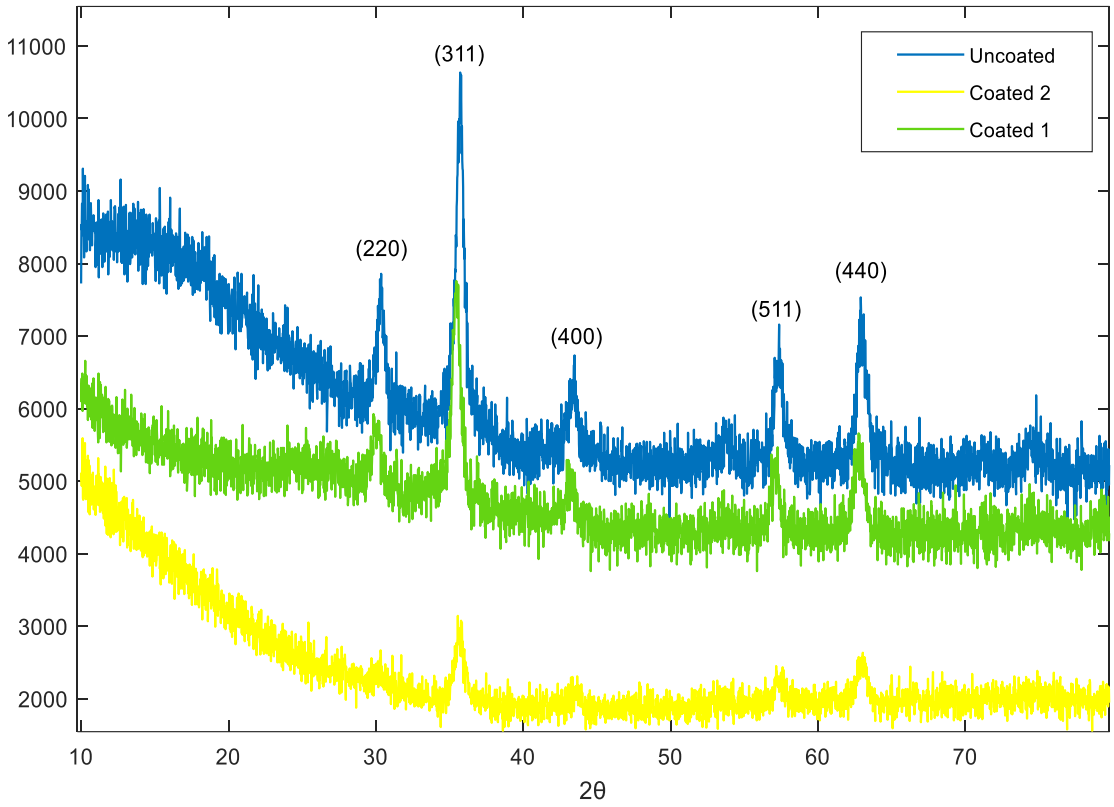

Figure 5.2: XRD patterns of MNP and SMNP

Table 5.1: Main XRD Peaks

2θ (Experiment)	2θ (Reference) JCPDS 19-0629 [42,44]	Miller Indices (Plane)
30.33	30.10	220
35.77	35.40	311
43.44	43.10	400
53.80	53.40	422
57.21	56.90	511
62.87	62.60	440

The obtained peak values are in good agreement with above reference and previously reported results [4, 6, 9,10, 31] and indicates pure Magnetite (Fe_3O_4) cubic inverse spinel structure [44]. The SMNPs XRD patterns show similar peaks which indicates that crystallinity of the core is

retained. The slightly shifted peak position in SMNPs and significantly reduced peak intensities indicate a good shell surrounds the magnetite core or formation of silica coated magnetite nanoparticles [12, 48]. The crystallite size (D_{XRD}), interplanar spacing (d_{hkl}), lattice parameter (a) are calculated for most prominent peaks (311), (511) and (440) of all samples using Scherrer formula and presented in Table 5.2.

Table 5.2: XRD Data Analysis

Plane	Size, D_{XRD} (nm)			d_{hkl} (Å)			a (Å)		
	Uncoated	Coated1	Coated2	Uncoated	C1	C2	Uncoated	C1	C2
311	13.76	13.43	10.47	2.51	2.53	2.51	8.32	8.40	8.34
511	11.48	15.72	9.25	1.61	1.61	1.60	8.36	8.37	8.32
440	10.52	12.41	13.04	1.48	1.48	1.47	8.35	8.37	8.34
avg	11.23	13.85	10.92						

The average (Major peaks) crystallite size is 11.23nm, 13.85nm, 10.92nm in uncoated, coated1 and coated2 sample respectively. The lattice constants are almost unchanged between uncoated and coated MNPs. These results are further discussed with TEM particle sizes in section 5.3

5.3 TEM and EDS Images:

The TEM images, EDS spectrum of uncoated , coated1 and coated2 sample are presented in figure 5.3, 5.4 and 5.5 respectively. The particles sizes of uncoated and coated samples are presented in Table 5.3.

Table 5.3: Particles sizes of Uncoated and Coated samples measured from TEM image

	Particle size				Coating Thickness
Sample	No of measurement	Mean, nm	Min, nm	Max, nm	Mean, nm
Uncoated	74	12.19±3.11	7.41	28.62	
Coated-1	84	14.23±2.79	9.41	20.03	1.76±0.48
Coated-2	43	12.22±2.97	8.05	19.15	1.34±0.39

The particles sizes are very near to the crystallite sizes calculated by XRD analysis, which indicates that overall uniform distribution or less agglomeration in all the samples. The uncoated particles are ranged between 7.41nm to 28.62nm averaging 12.19±3.11nm. The average coating thickness were found 1.76±0.48nm and 1.34±0.39nm for coated1 and coated2 samples. Although the particles size is not much changed in uncoated and coated sample but still there is better uniform distribution in silica coated samples. (ranges 9.41 to 20.43nm in coated1 and 8.05 to 19.15nm in coated2). In some previous results [3, 10, 11] reported (presented in table 2.4) that, they found much larger particle size and crystallite size in coated sample because of the agglomeration of MNPs inside the nanosphere which is not happened in this study. So, the results of this work indicate almost no agglomeration in the coated samples. The coated1 sample (prepared by sol-gel and magnetic stirring) has little bit higher size (both in XRD and TEM) than uncoated which is

well matched with previous results of sol-gel synthesis reported by Farimani et al. 2013 [44] and coprecipitation synthesis reported by Wang et al. 2010 [34]. The almost unchanged particles size and very little less crystallite size of coated 2 sample (prepared by ultrasonic stirring) indicates, the particle is not damaged in high ultrasonic field and show even better uniform coating of each particle. The faster hydrolysis of TEOS in ultrasonic field than magnetic/mechanical stirring (slower hydrolysis process) may be the contributing factor for these small differences in results [20]. The decrease in crystallite size may be also happened due to the lattice contraction and macrostrain enhancement of Fe_3O_4 due to SiO_2 coating [41].

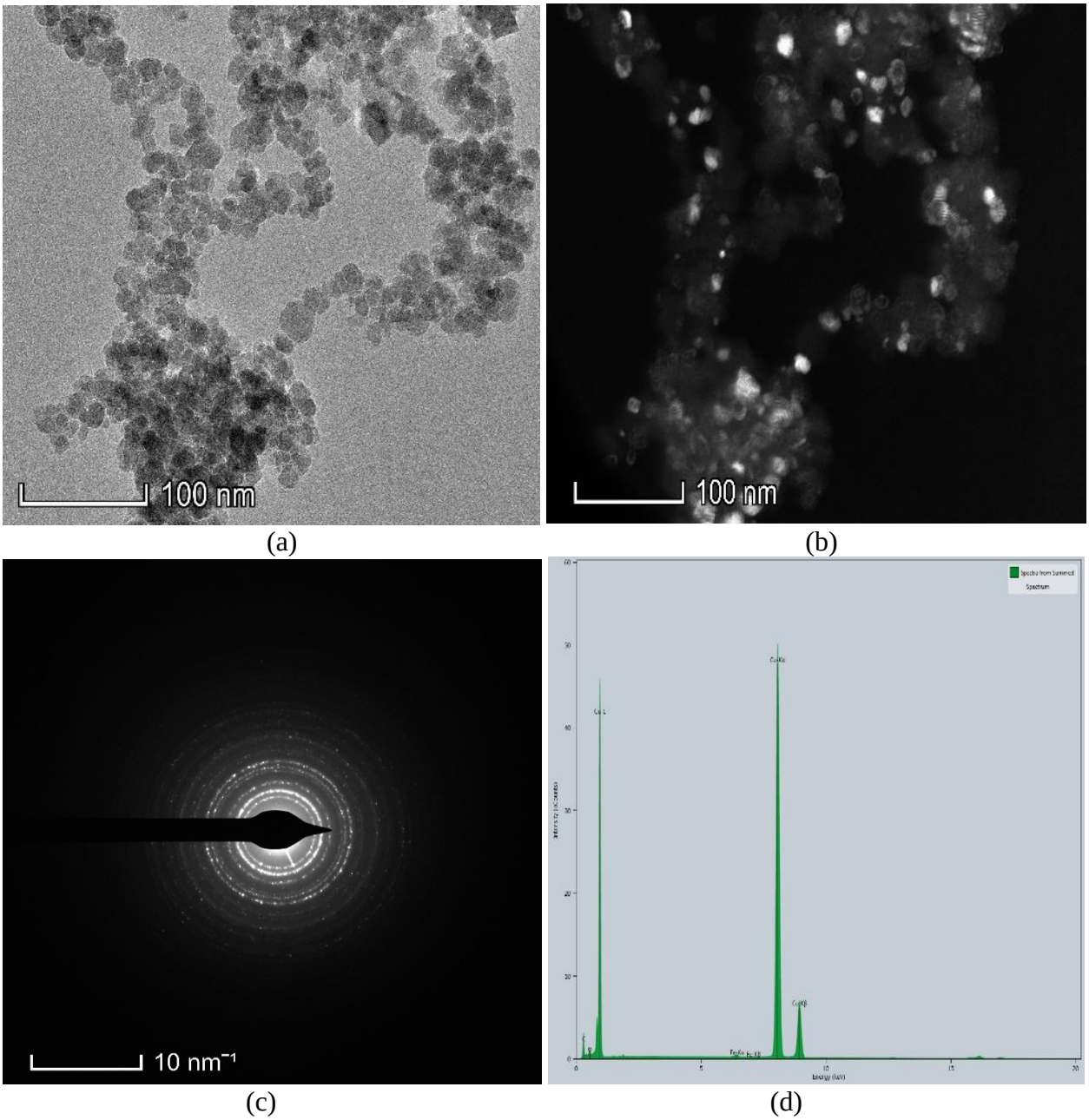

(a) (b)

(c) (d)

Figure 5.3: TEM Images of Uncoated MNP - (a) Bright field (b) Dark field (c) SAED Pattern (d) EDS spectrum

The prominent SAED (Selected area electron diffraction) rings comes from the planes (220), (311), (400), (422), (511), (440) (shown in Figure 5.3c and 5.4a) for both MNP and SMNP, confirms the excellent crystallinity of cubic Fe_3O_4 without presenting any other phase.

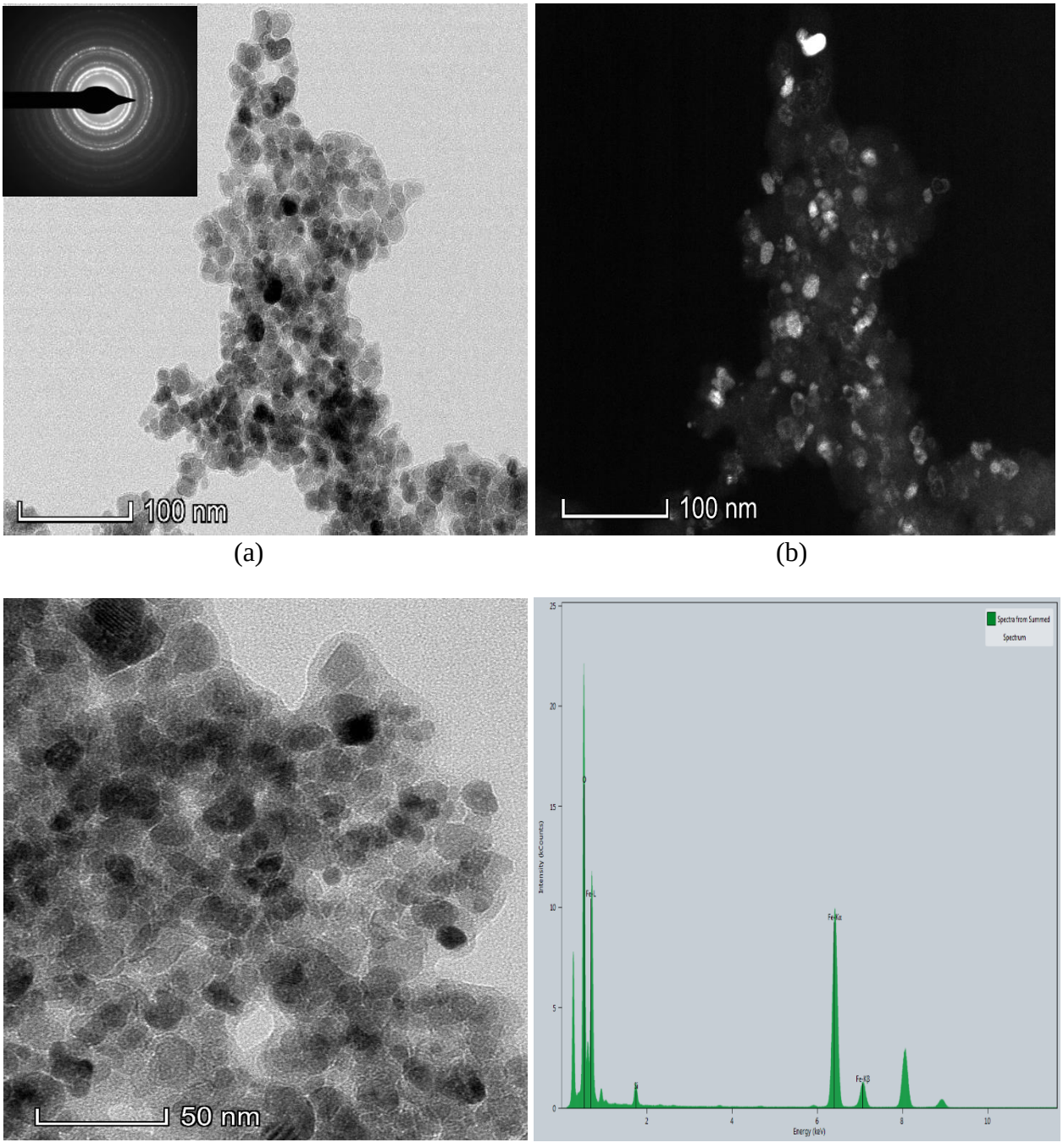

(a) (b)

(c) (d)

Figure 5.4: TEM Images of Coated1 MNP - (a & c) Bright field and SAED pattern (b) Dark field (d) EDS spectrum

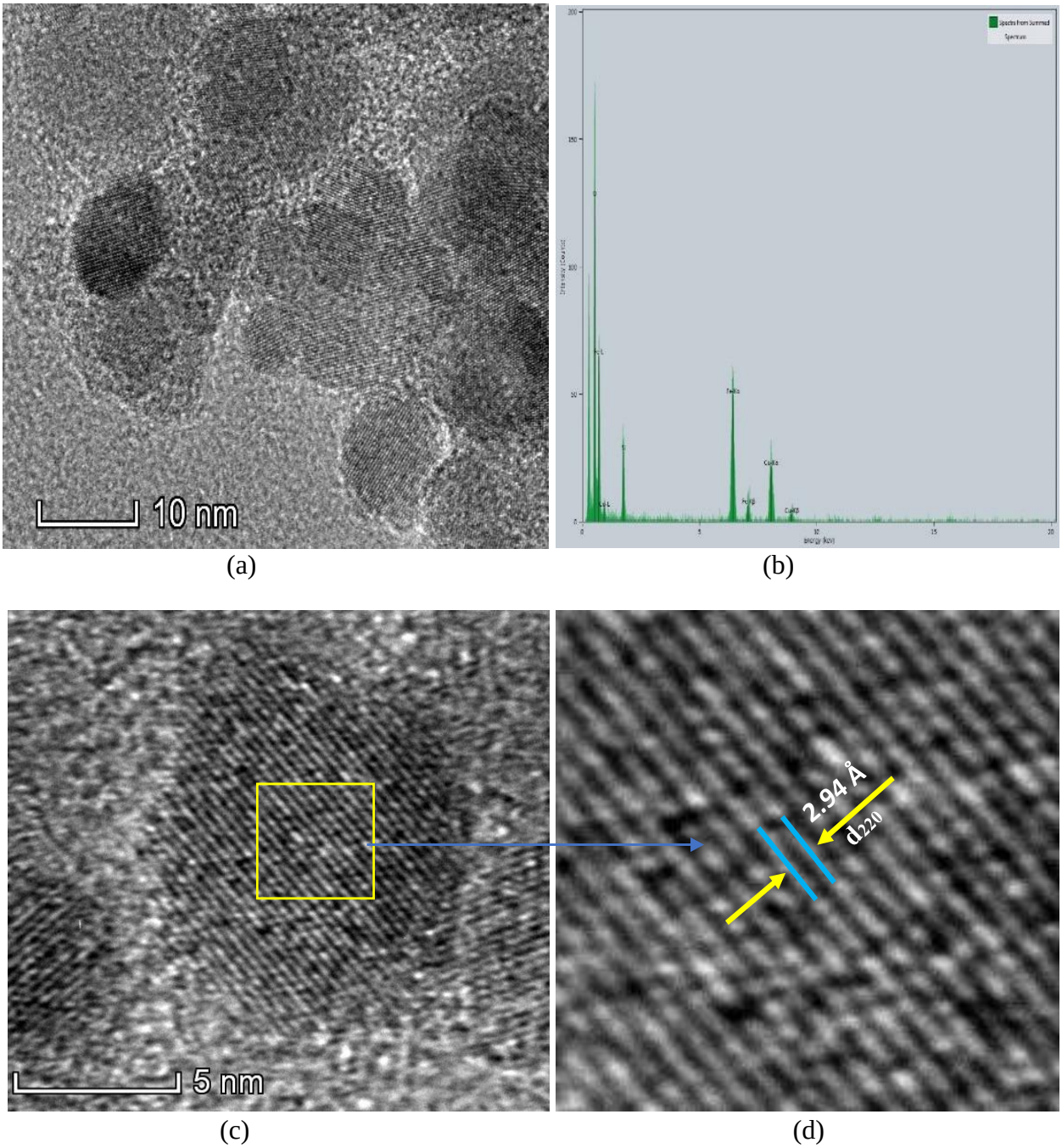

(a) (b)

(c) (d)

Figure 5.5: HRTEM Images of Coated2 MNP – (a & c) Crystallite, (b) EDS spectrum, (d) d_{hkl}

The HRTEM analysis of coated2 sample presents the excellent crystallite distributions with almost no agglomeration (figure 5.5a & 5.5c). A single crystallite of 9.935nm size with 0.294nm interplanar distance corresponds to the (220) plane of Fe_3O_4 core is presented in figure 5.5c & d.

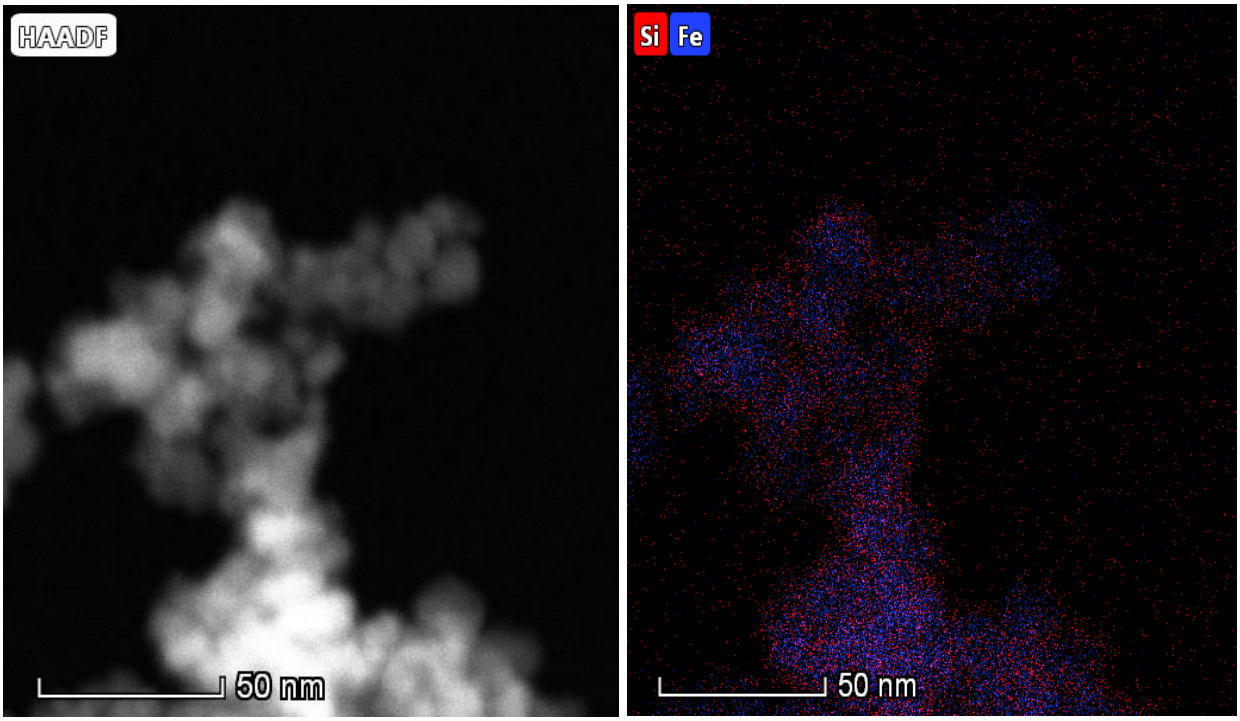

Figure 5.6: EDS Mapping of Coated2 MNP

The silica coating is further analyzed by EDS mapping of Coated2 sample shown in figure 5.6. The blue and red color indicates the Fe and Si elements representing Fe_3O_4 core and SiO_2 shell. It indicates uniform particle distributions and shows almost every MNP is coated by Silica. The uniform coating distribution with higher surface area should provide better adsortion efficiency for the heavy metal/radionuclides seperation.

5.4 Raman Spectra:

The uncoated and coated MNP were further characterized by Raman spectroscopy. The sharpest peak found at 625, 564, 451 and 386 cm^{-1} (figure 5.7) are the probable characteristics Fe-O stretching and vibrational bonds of Fe_3O_4 [41, 63, 64]. Depending on the Laser wavelength used the values can be shifted as reported by Panta & Bargmann (2015) [49]. There are some other peaks also appeared in the spectrum of uncoated sample, most probably due to the oxidation happened during the Raman experiment which was also reported by Panta & Bargmann (2015) and Yew et al. (2017) [63] or may be cosmic effect. Instead of sharp oxidation band near 200-210 cm^{-1} region in uncoated sample (probable oxidation peak), a wider peak is found near 210 cm^{-1} and most probably small wider peaks at 378 and 470 cm^{-1} are the peaks of silica [41]. The reduced intensities and slightly shifted Fe-O bonds in the coated sample are indicatives of the coating of magnetite nanoparticles by silica which was also reported by Majumder et al. (2015).

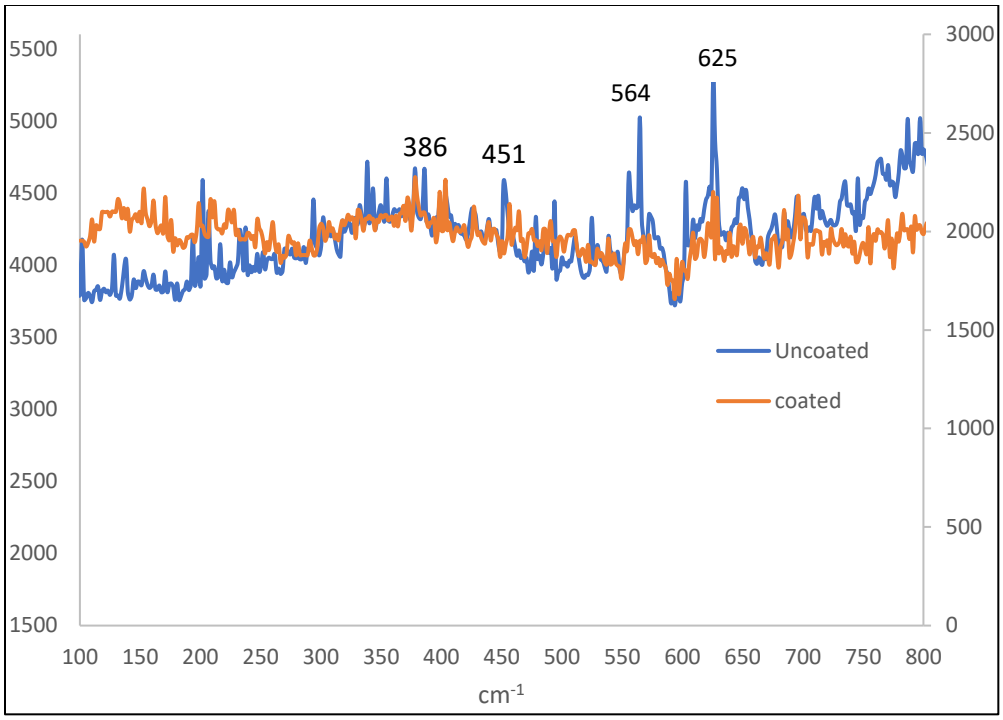

Figure 5.7: Raman spectra of uncoated and coated sample

5.5 DSC and TGA Curves:

The DSC and TGA curves of uncoated and coated MNPs are presented in figure 5.8a, 5.8b and 5.8c.

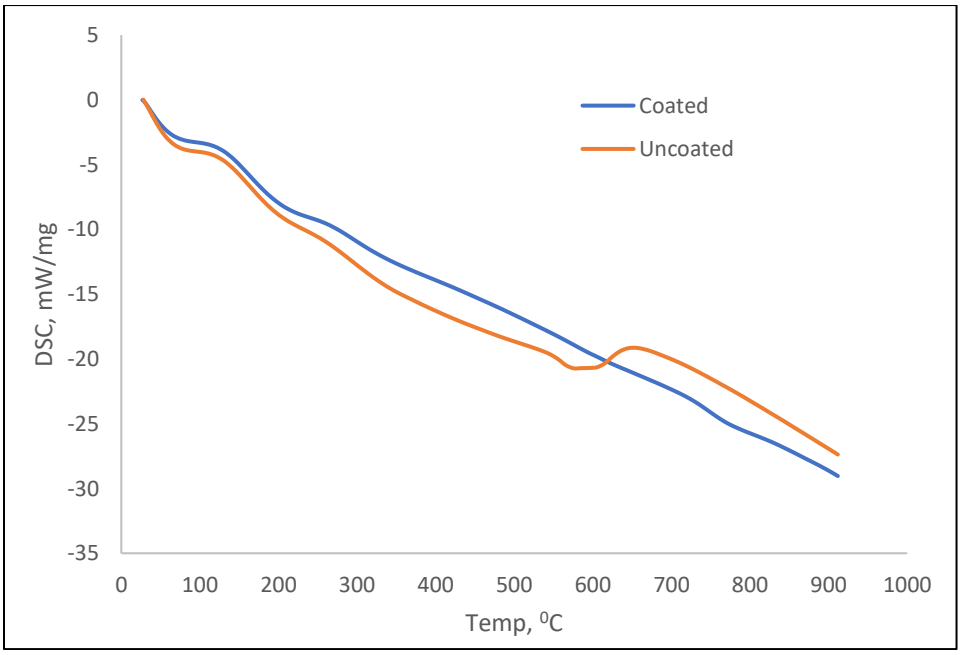

(a)

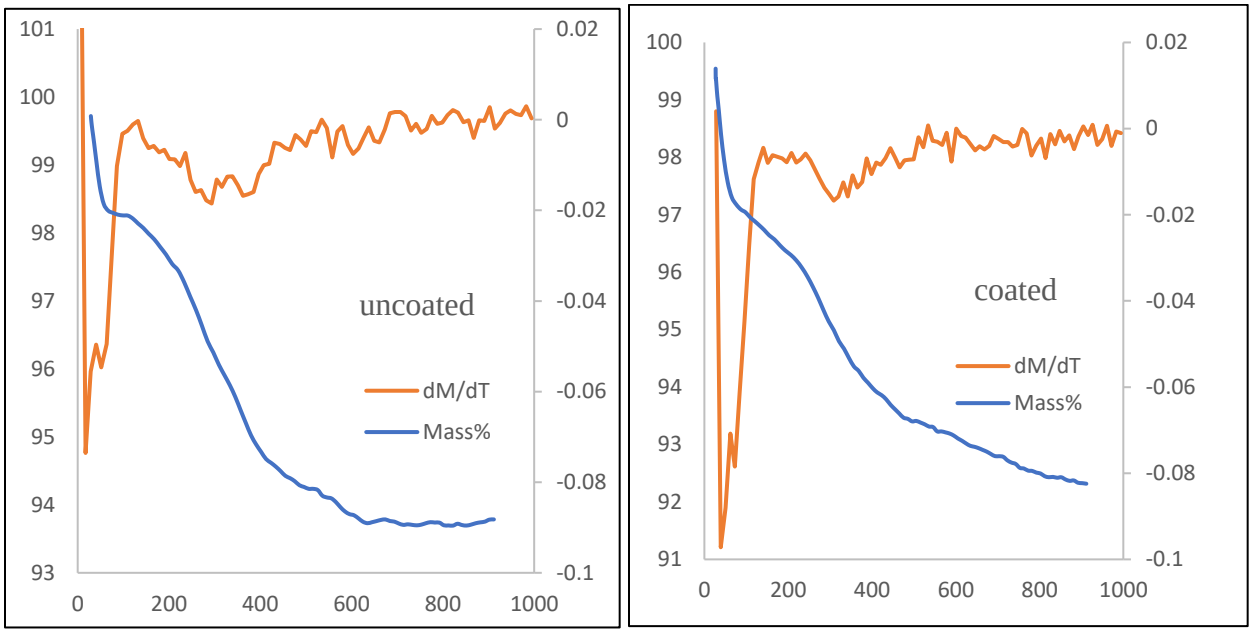

(b) (c)

Figure 5.8: DSC and TGA curves of coated and uncoated MNP- a. DSC, b. TGA_uncoated c. TGA_coated

The endothermic peaks in figure 5.8a around 90^0C for both uncoated and coated indicate the removal of water and around 150-350^0C removal and decomposition of residual chemicals/substances on the surface of Uncoated and Coated MNPs. This information is in line with TGA curves (mass% and dM/dT plots) shown in figure 5.8b & 5.8c, which show rapid weight loss (5-6%) around 100-300^0C. For uncoated MNP, another endothermic peak in DSC curve with little mass loss in TGA curve around 590-610^0C may be due to the phase transition of Fe_3O_4 to FeO [29]. This peak was not found in coated sample, so most probably the silica coat prevents the phase transition of Magnetite that means thermal stability is increased in SMNP. the Coated MNPs show slightly more weight loss initially than uncoated because of decomposition/evaporation of more surface water, chemical/ethanol content. The weight loss from 400^0C to 900^0C is not that significant, which confirms the good thermal stability of SMNP up to this temperature.

5.6 Magnetic Properties:

The hysteresis loops of magnetite from 5K to 400K is presented in figure 5.9. It is clearly seen that the coercivity and remanence are very low which indicates the superparamagnetic nature of the synthesized nanoparticles. Although the hysteresis window is very low for all the temperatures (5K-400K) shown in figure 5.9a, the hysteresis window become more narrower with the increasing temperature in the magnified image shown in figure 5.9b and values in Table 5.4. So, the superparamagnetic behavior is increasing with temperature and around the room temperature(300K), magnetite became perfectly superparamagnetic [72]. The increasing magnetic

anisotropy with increasing temperature is the reason for the increasing superparamagnetic behavior. The exact values of saturation magnetization (Ms), Coercivity (Hc) and anisotropy constant, k is calculated following the Néel k, the magnetic energy barrier, Hc = 2k/Ms [76] at some of the selected temperatures are presented in Table 5.4.

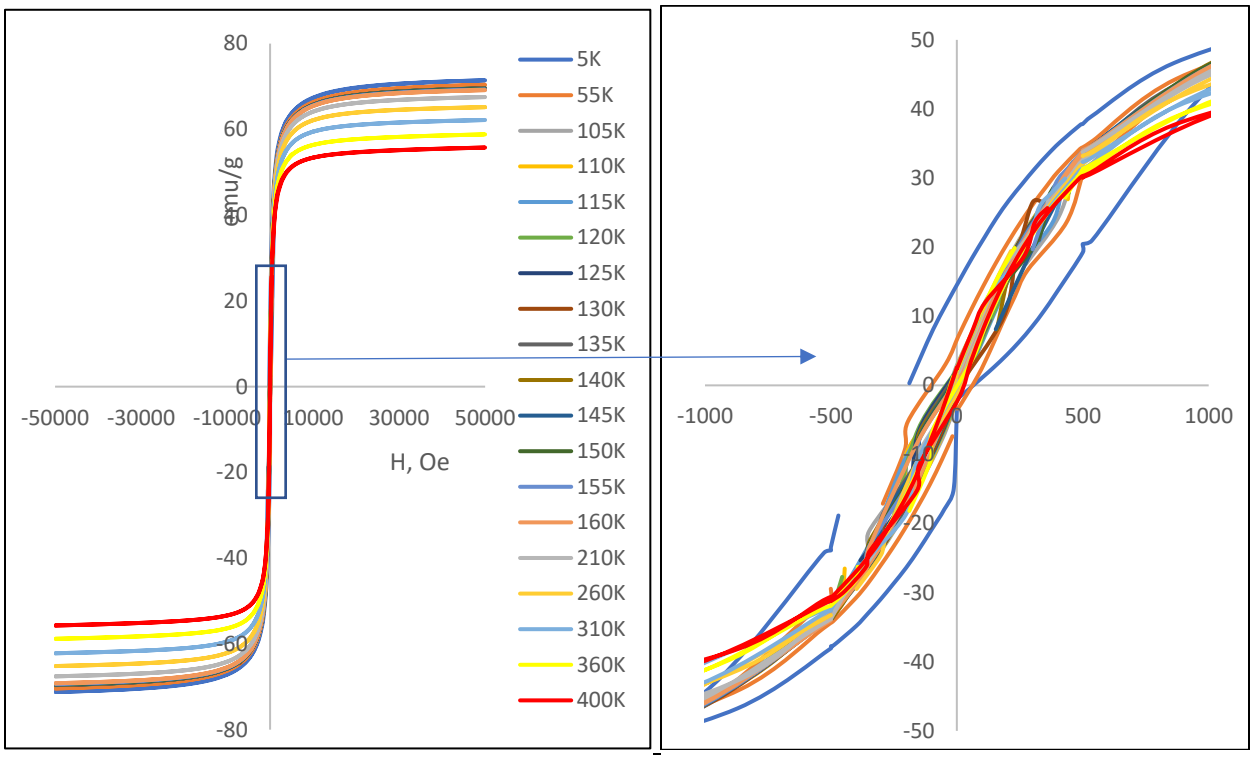

Figure 5.9: Hysteresis loop of MNP at different Temperatures

Table 5.4: Ms and Hc values of Magnetite

Temperature, K	Saturation Magnetization, Ms (emu/g)	Coercivity, Hc (Oe)	Anisotropy Constant, k (=Ms*Hc/2)
5	71.44	193.14	6898.96
55	70.39	100.02	3520.20
110	69.55	30.96	1076.63
115	69.53	26.61	925.09
120	69.58	40.54	1410.38
125	69.56	37.28	1296.59
130	69.54	25.37	882.114

Temperature, K	Saturation Magnetization, Ms (emu/g)	Coercivity, Hc (Oe)	Anisotropy Constant, k (=Ms*Hc/2)
135	69.53	31.39	2182.55
210	67.53	7.4	249.86
310	62.19	4.87	151.43
360	58.82	3.76	221.16

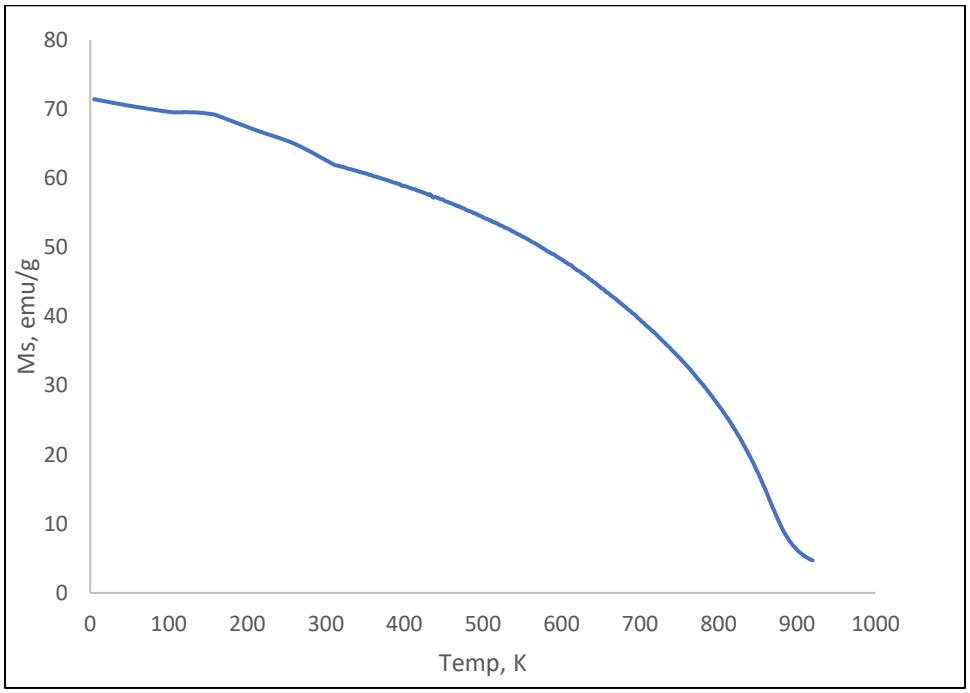

Figure 5.10: Saturation Magnetization of MNP vs Temperature

The decreasing Ms, Hc, and k with increasing temperature (as shown in figure 5.10, 5.11a and table 5.4) follow the same trend except the region around 120K, where there is sudden increase of Ms and Hc happened. This is due to the Verwey Transition (Tv) which reported by many other earlier findings mainly near 120-130K [72, 74]. In our case, the transition is not so prominent or small increase in Ms and Hc value is most probably due to small particle sizes (12.19±3.11nm) as it was mentioned earlier that, below 20nm particle size, Verwey effect becomes suppressed and below 6nm completely disappeared (Bohra, Agarwal & Singh, 2108) [74]. Although the exact explanation of Verwey transition still not concrete, the most probable reason stated by the researchers (as cited by Hu et al. 2018) are may be the changed charged-ordered structures of Fe^{3+} and Fe^{2+} and the lattice distortions of the cubic structure [72]. Coercivity increased sharply with increasing field as shown in figure 5.11b as the rapid change in anisotropy initially with external applied field until reaches the saturation point.

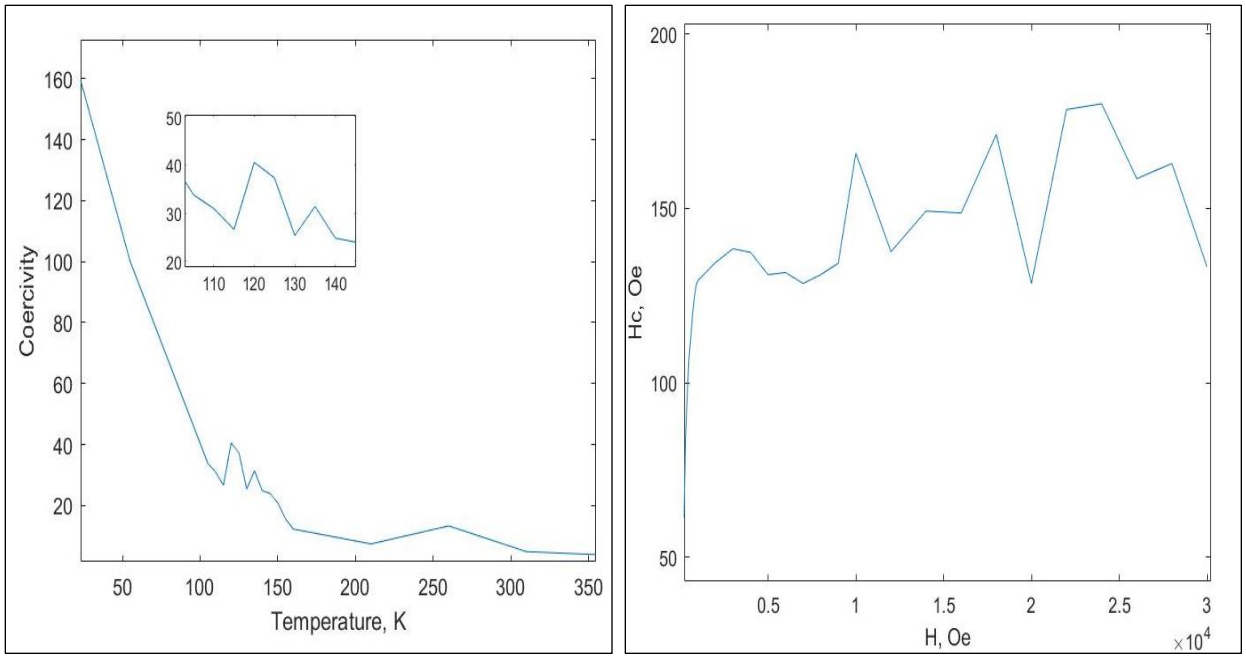

(a) (b)

Figure 5.11: Temperature (a) and Field (b) dependent coercivity of MNP

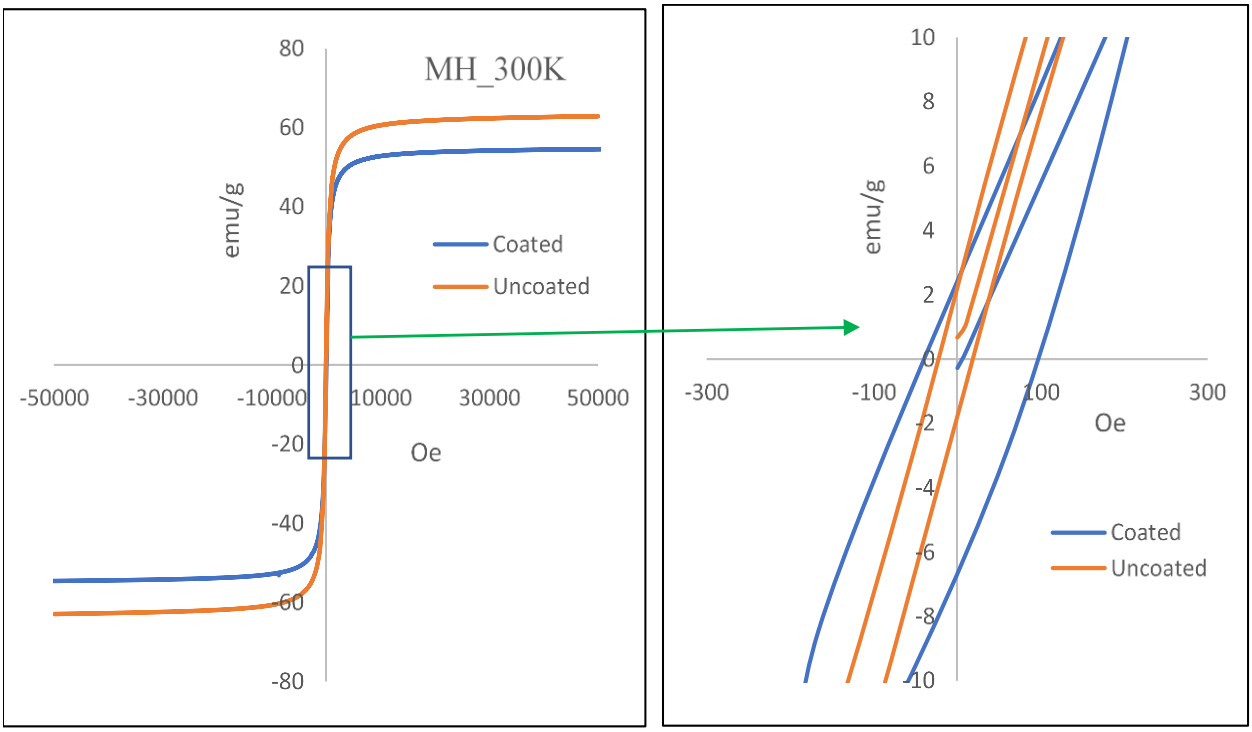

Figure 5.12: Magnetic Properties of SMNP at 300K

The change in magnetic properties due to the silica coating on MNPs is reported at room temperature (300K) in figure 5.12. The Ms of coated sample (54.5 emu/g) is expectedly lower than the uncoated sample (62.9 emu/g) and Hc of coated sample slightly higher than the uncoated sample. The very narrow hysteresis window indicate that the coated sample still retain the superparamagnetic nature of the bare Magnetite. The decrease in magnetization of the coated sample is due to the formation of Fe-O-Si bond upon silica coating which increases the surface spin disorder and the silica surface reduces the magnetic dipole-dipole interactions in coated MNPs [70, 75]. The Magnetic properties of the MNP and SMNP confirms that they can be separated very easily by magnetic forces after adsorption of heavy metals/radionuclides from aqueous solution.

6. Conclusion:

The main findings of the thesis work carried out are pointed out below:

- All the nanoparticles (uncoated and coated) were synthesized successfully.
- The FTIR spectra, x-ray and electronic diffraction patterns, crystallite images confirmed the presence of the high purity single phase Fe_3O_4 nanoparticles with inverse spinel cubic structure.
- The reduced intensities and shifted magnetite characteristics peak positions in FTIR spectra, X-ray diffraction pattern, Raman spectra and moreover, EDS mapping in TEM for elemental position of Fe and Si confirmed the formation of Fe-O-Si bond or formation of core-shell structure of Fe_3O_4/SiO_2 nanoparticles.
- The average particle sizes measured manually from TEM images were 12.19±3.11nm, 14.23±2.79nm and 12.22±2.97nm for uncoated, coated1 and coated2 samples with average coating thickness of 1.76±0.48nm and 1.34±0.39nm for coated1 and coated2 sample respectively.
- Successful synthesis of both coated samples with uniform particle size distributions and not much evidence of blank silica spheres validated the optimization in use of chemical reagents and synthesis procedure followed. Although a little bit more TEOS concentration can be used to increase the silica coating thickness little bit for more surface stability.
- The little bit better particles uniformity and slightly lower crystallite size of coated2 samples can be attributed to use of high-power ultrasonic stirring which provided the faster hydrolysis of TEOS and prevent agglomeration. Although pretreatment with HCL done in coated1 synthesis done by magnetic stirring also prevent large agglomeration. To understand better and observe the difference between mechanical/magnetic stirring and ultrasonic stirring effect, some more works need to done with keeping all other variables unchanged.
- The oxidations/phase transition of Fe_3O_4 observed in Raman spectroscopy and DSC analysis is suppressed in coated sample, so most probably the silica coating protects the magnetite core from oxidation/phase transition or provide better thermal stability.
- The temperature dependent hysteresis loops of Magnetite nanoparticles revealed the better superparamagnetic behavior near Room temperature.
- The Verwey transition effect was observed near 120K, although not so prominent because of the size effect (less than 20nm) of nanoparticles in this case.
- Although the saturation magnetization was decreased in coated sample but still, they showed enough superparamagnetic properties for easy magnetic separation from solution.

It can be concluded that, the large surface area given by the fact of very smaller particles with uniform size distributions, formation of protective silica layer with presence of hydroxyl groups for easy conjugation with further application specific functional groups if needed and superparamagnetic properties of these synthesized nanoparticles make them potential candidates to be used for separation of toxic heavy metals/radionuclides from contaminated aqueous medium.
.

References

1. Mahmoudi M, Sant S, Wang B, Laurent S, Sen T. Superparamagnetic iron oxide nanoparticles (SPIONs): development, surface modification and applications in chemotherapy. Adv Drug Deliv Rev. 2011;63(1-2):24-46. doi: 10.1016/j.addr.2010.05.006

2. Pragnesh N. Dave, Lakhan V. Chopda. Application of Iron Oxide Nanomaterials for the Removal of Heavy Metals. Article ID 398569, 2014, https://doi.org/10.1155/2014/398569.

3. Glaria, A. & Soulé, Samantha & Hallali, Nicolas & Ojo, W.-S & Mirjolet, M. & Fuks, Gad & Cornejo, Alfonso & Allouche, Joachim & Dupin, Jean-Charles & Martinez, Herve & Carrey, Julian & Chaudret, Bruno & Delpech, Fabien & Lachaize, S. & Nayral, Céline. (2018). Silica coated iron nanoparticles: Synthesis, interface control, magnetic and hyperthermia properties. RSC Advances. 8. 32146-32156. 10.1039/C8RA06075D.

4. Lee, Dae-Won & Fatima, Hira & Kim, Kyo-Seon. (2018). Preparation of Silica Coated Magnetic Nanoparticles for Bioseparation. Journal of Nanoscience and Nanotechnology. 18. 1414-1418. 10.1166/jnn.2018.14888.

5. Gao Z, Ring HL, Sharma A, Namsrai B, Tran N, Finger EB et al. Preparation of Scalable Silica-Coated Iron Oxide Nanoparticles for Nanowarming. Advanced Science. 2020 Feb 1;7(4). 1901624. https://doi.org/10.1002/advs.201901624

6. Pasandideh, Elahe & Kakavandi, Babak & Nasseri, Simin & Mahvi, Amir & Nabizadeh, Ramin & Esrafili, Ali & Rezaei Kalantary, Roshanak. (2016). Silica-coated magnetite nanoparticles core-shell spheres (Fe3O4@SiO2) for natural organic matter removal. Journal of Environmental Health Science and Engineering. 14. 10.1186/s40201-016-0262-y.

7. Xiang, Guoqiang & Li, Lulu & Jiang, Xiuming & He, Lijun & Fan, Lu. (2013). Thio Modified Magnetic Silica Sorbent for the Determination of Trace Mercury in Environmental Water Samples Coupled with Cold Vapor Atomic Absorption Spectrometry. Analytical Letters. 46. 10.1080/00032719.2012.726679.

8. Fan, Qingqian & Guan, Yueping & Zhang, Zhi & Xu, Guoli & Yang, Yu & Guo, Chen. (2018). A new method of synthesis weldispersion and dense Fe3O4@SiO2 magnetic nanoparticles for DNA extraction. Chemical Physics Letters. 715. 10.1016/j.cplett.2018.11.001.

9. Shao, Huiping & Qi, Jiangcong & Lin, Tao & Yuling, Zhou. (2017). Preparation and Characterization of Fe 3 O 4 @SiO 2 @NMDP core-shell structure composite magnetic nanoparticles. Ceramics International. 44. 10.1016/j.ceramint.2017.10.184.

10. Esmaeilpour, Mohsen & Sardarian, Alireza & Javidi, Jaber. (2012). Schiff base complex of metal ions supported on superparamagnetic Fe3O4@SiO2 nanoparticles: An efficient, selective and recyclable catalyst for synthesis of 1,1-diacetates from aldehydes under solvent-free conditions. Applied Catalysis A: General. s 445–446. 359–367. 10.1016/j.apcata.2012.09.010.

11. Asab, Goshu & Zereffa, E. & Seghne, Teshome. (2020). Synthesis of Silica-Coated Fe 3 O 4 Nanoparticles by Microemulsion Method: Characterization and Evaluation of Antimicrobial Activity. International Journal of Biomaterials. 2020. 1-11. 10.1155/2020/4783612.

12. Noval Lara, Virginia & Carriazo, José. (2019). Fe3O4-TiO2 and Fe3O4-SiO2 Core-shell Powders Synthesized from Industrially Processed Magnetite (Fe3O4) Microparticles. Materials Research. 22. 10.1590/1980-5373-mr-2018-0660.

13. Werner Stöber, Athur Fink. Controlled Growth of Monodisperse Silica Spheres in the Micron Size Range. Journal of colloid and interface science 26, 62-69 (1968).

14. Ali A, Zafar H, Zia M, Ul Haq I, Phull AR, Ali JS, Hussain A. Synthesis, characterization, applications, and challenges of iron oxide nanoparticles. Nanotechnol Sci Appl. 2016 Aug 19;9:49-67. doi: 10.2147/NSA.S99986. PMID: 27578966; PMCID: PMC4998023.

15. Van Quy, Dao & Minh Hieu, Nguyen & Tra, Pham & Nam, Nguyen & Nguyen, Hoang & Son, Nguyen & Phan, Tuan-Nghia & Anh, Nguyen & Hong, Tran & Luong, Nguyen. (2013). Synthesis of Silica-Coated Magnetic Nanoparticles and Application in the Detection of Pathogenic Viruses. Journal of Nanomaterials. 2013. 10.1155/2013/603940.

16. Zeinab Sharafia , Bita Bakhshib , Jaber Javidic and Sina Adrangi. Synthesis of Silica-coated Iron Oxide Nanoparticles: Preventing Aggregation without Using Additives or Seed Pretreatment. Iranian Journal of Pharmaceutical Research (2018), 17 (1): 386-395.

17. Jamali-Behnam, Farideh & Najafpoor, Ali Asghar & Davoudi, Mojtaba & Rohani Bastami, Tahereh & Alidadi, Hossein & Esmaily, Habibollah & Dolatabadi, Maryam. (2017). Adsorptive removal of arsenic from aqueous solutions using magnetite nanoparticles and silica-coated magnetite nanoparticles. Environmental Progress & Sustainable Energy. 10.1002/ep.12751.

18. Pham, Xuan-Hung & Eunil, Hahm & Kim, Hyung-Mo & Son, Byung & Jo, Ahla & An, Jaehyun & Thi, Tuong & Nguyen, Quan & Jun, Bong-Hyun. (2020). Silica-Coated Magnetic Iron Oxide Nanoparticles Grafted onto Graphene Oxide for Protein Isolation. Nanomaterials. 10. 117. 10.3390/nano10010117.

19. Deng, Yonghui & Wang, C.C & Hu, J.-H & Yang, Wuli & Fu, S.-K. (2005). Investigation of formation of silica-coated magnetite nanoparticles via sogel approach. Colloids and Surfaces a-Physicochemical and Engineering Aspects. 262. 87-93. 10.1016/j.colsurfa.2005.04.009.

20. Anne-Laure, Morel & Nikitenko, Sergey & Gionnet, Karine & Wattiaux, Alain & Lai Kee Him, Joséphine & Labrugere, Christine & Chevalier, Bernard & Deleris, Gerard & Petibois, Cyril & Brisson, Alain & Simonoff, Monique. (2008). Sonochemical Approach to the Synthesis of Fe 3 O 4 @SiO 2 Core−Shell Nanoparticles with Tunable Properties. ACS nano. 2. 847-56. 10.1021/nn800091q.

21. Hui, Chao & Shen, Chengmin & Tian, Jifa & Bao, Lihong & Ding, Hao & Li, Chen & Tian, Yuan & Xuezhao, Shi & Gao, Hong-Jun. (2011). Core-shell Fe3O4@SiO2 nanoparticles synthesized with weldispersed hydrophilic Fe3O4 seeds. Nanoscale. 3. 701-5. 10.1039/c0nr00497a.

22. Wu, Shen & Sun, Aizhi & Lu, Zhenwen & Cheng, Chuan & Gao, Xuexu. (2015). Magnetic properties of iron-based soft magnetic composites with SiO2 coating obtained by reverse microemulsion method. Journal of Magnetism and Magnetic Materials. 381. 451-456. 10.1016/j.jmmm.2015.01.030.

23. Wu, Shen & Sun, Aizhi & Lu, Zhenwen & Cheng, Chuan & Gao, Xuexu. (2015). Magnetic properties of iron-based soft magnetic composites with SiO2 coating obtained by reverse microemulsion method. Journal of Magnetism and Magnetic Materials. 381. 451-456. 10.1016/j.jmmm.2015.01.030.

24. Nath D. (2018) Nanomaterial for the Management of Radioactive Waste. In: Martínez L., Kharissova O., Kharisov B. (eds) Handbook of Ecomaterials. Springer, Cham. https://doi.org/10.1007/978-3-319-48281-1_49-1.

25. N, Meenakshi sundaram & Murugesan, Sneha. (2015). Preparation and characterization of an iron oxide-hydroxyapatite nanocomposite for potential bone cancer therapy. International Journal of Nanomedicine. 10. 99. 10.2147/IJN.S79985.

26. Iqbal, M. Zubair & Ma, Xuehua & Chen, Tianxiang & Zhang, Linge & Ren, Wenzhi & Xiang, Lingchao & Wu, Aiguo. (2015). Silica Coated Super-paramagnetic Iron Oxide Nanoparticles (SPIONPs): A New Type Contrast Agent of T1 Magnetic Resonance Imaging (MRI). J. Mater. Chem. B. 3. 10.1039/C5TB00300H.

27. Ahangaran, Fatemeh & Hassanzadeh, Ali & Nouri, Sirous. (2013). Surface modification of Fe3O4@SiO2 microsphere by silane coupling agent. International Nano Letters. 3. 10.1186/2228-5326-3-23.

28. Lewandowska, Joanna & Staszewska, Magdalena & Kepczynski, Mariusz & Szuwarzyński, Michał & Łatkiewicz, Anna & Olejniczak, Zbigniew & Nowakowska, Maria. (2012). Sol–gel synthesis of iron oxide–silica composite microstructures. Journal of SoGel Science and Technology. 64. 67-77. 10.1007/s10971-012-2828-1.

29. Aghazadeh, Mustafa & Karimzadeh, Isa & Ganjali, Mohammad. (2019). Dextran grafted nickedoped superparamagnetic iron oxide nanoparticles: Electrochemical synthesis and characterization. 9. 531-538. 10.22052/JNS.2019.03.014.

30. Khoobi, Mehdi & Motevalizadeh, Seyed & Asadgol, Zahra & Forootanfar, Hamid & Faramarzi, Mohammad. (2015). Polyethyleneimine-modified superparamagnetic Fe3O4 nanoparticles for lipase immobilization: Characterization and application. Materials Chemistry and Physics. 149-150. 77-86. 10.1016/j.matchemphys.2014.09.039.

31. Wang, Dong & Guan, Kaiwen & Bai, Zhiping & Liu, Fuqiang. (2016). Facile preparation of acid-resistant magnetite particles for removal of Sb(III) from strong acidic solution. Science and Technology of Advanced Materials. 17. 1-9. 10.1080/14686996.2016.1145530.

32. Madrakian, Tayyebeh & Afkhami, Abbas & Zolfigol, Mohammad Ali & Ahmadi, Mazaher & Koukabi, Nadia. (2012). Application of Modified Silica Coated Magnetite Nanoparticles for Removal of Iodine from Water Samples. nano-micro letters. 4. 57-63. 10.3786/nml.v4i1.p57-63.

33. Park, Sung & Kim, Ki & Kim, Hee Taik. (2002). Preparation of silica nanoparticles: Determination of the optimal synthesis conditions for small and uniform particles. Colloids and Surfaces A: Physicochemical and Engineering Aspects. 197. 7–17. 10.1016/S0927-7757(01)00683-5.

34. Wang J, Zheng S, Shao Y, et al. Amino-functionalized Fe(3)O(4)@SiO(2) core-shell magnetic nanomaterial as a novel adsorbent for aqueous heavy metals removal. Journal of Colloid and Interface Science. 2010 Sep;349(1):293-299. DOI: 10.1016/j.jcis.2010.05.010.

35. Lien, yi-hsin & Wu, Tzong-Ming. (2008). Preparation and characterization of thermosensitive polymers grafted onto silica-coated iron oxide nanoparticles. Journal of colloid and interface science. 326. 517-21. 10.1016/j.jcis.2008.06.020.

36. Chen, Fei-Hu & Gao, Q & Ni, J. (2008). The grafting and release behavior of doxorubincin from Fe3O 4@SiO2 core-shell structure nanoparticles via an acid cleaving amide bond: The potential for magnetic targeting drug delivery. Nanotechnology. 19. 165103. 10.1088/0957-4484/19/16/165103.

37. Lesiak B, Rangam N, Jiricek P, Gordeev I, Tóth J, Kövér L, Mohai M, Borowicz P. Surface Study of Fe3O4 Nanoparticles Functionalized With Biocompatible Adsorbed Molecules. Front Chem. 2019 Oct 4;7:642. doi: 10.3389/fchem.2019.00642. PMID: 31637230; PMCID: PMC6787174.

38. Dukenbayev, Kanat & Korolkov, Ilya & Chushkova, Darya & Kozlovskiy, Artem & Trukhanov, Sergei & Gorin, Yevgeniy & Shumskaya, Alena & Kaniukov, Egor & Vinnik, Denis & Zdorovets, M. & Anisovich, Maryna & Trukhanov, A. & Tosi, Daniele & Molardi, Carlo. (2019). Fe3O4 Nanoparticles for Complex Targeted Delivery and Boron Neutron Capture Therapy. Nanomaterials. 9. 494. 10.3390/nano9040494.

39. Soares, Sofia & Fernandes, Tiago & Trindade, Tito & Danieda-Silva, Ana Luísa. (2019). Trimethyl Chitosan/Siloxane-Hybrid Coated Fe3O4 Nanoparticles for the Uptake of Sulfamethoxazole from Water. Molecules. 24. 1958. 10.3390/molecules24101958.

40. Girginova, Penka & Danieda-Silva, Ana Luísa & Lopes, Cláudia & Figueira, Paula & Otero, Marta & Amaral, Vitor & Pereira, Eduarda & Trindade, Tito. (2010). Silica coated magnetite particles for magnetic removal of Hg2+ from water. Journal of colloid and interface science. 345. 234-40. 10.1016/j.jcis.2010.01.087.

41. Majumder, Sumit & Dey, Subhrajyoti & Bagani, Kousik & Dey, Sanjoy & Banerjee, Sangam & Kumar, Sanjay. (2015). A comparative study on structural, optical and magnetic properties of Fe3O4 and Fe3O4@SiO2 core-shell microspheres along with assessment of their potentiality as electrochemical double layer capacitor. Dalton Trans.. 44. 10.1039/C4DT02551B.

42. Munasir, M. & Dewanto, A. & Kusumawati, Diah & Putri, Nugrahani Primary & Yulianingsih, A. & Sa'adah, I. & Taufiq, Ahmad & Hidayat, Nurul & Sunaryono, Sunaryono & Supardi, Zainul. (2018). Structure Analysis of Fe 3 O 4 @SiO 2 Core Shells Prepared from Amorphous and Crystalline SiO 2 Particles. IOP Conference Series: Materials Science and Engineering. 367. 012010. 10.1088/1757-899X/367/1/012010.

43. Du, Guan-Hua & Liu, Z. & Xia, X. & Chu, Qian & Zhang, S.. (2006). Characterization and application of Fe3O4/SiO2 nanocomposites. Journal of SoGel Science and Technology. 39. 285-291. 10.1007/s10971-006-7780-5.

44. Helmi, M. & Farimani, R. & Shahtahmassebi, Nasser & Rezaee Roknabadi, Mahmood & Ghows, Narges. (2013). N. Ghows,Synthesis and study of structural and magnetic properties of super paramagnetic Fe3O4SiO2 core/shell nanocomposite for biomedical applications. Nanomed. J.. 1. 71-78.

45. Alam, M.N. (2002). Issues and trends in radioactive waste management in the perspectives of Bangladesh (IAEA-CN--90). International Atomic Energy Agency (IAEA)

46. Yunusa, Suleiman & Ahmed, Abdulkarim & Bawa, S.G. & Iyun, J.F. & Dauda, Mohammed. (2016). Preparation of High Grade Silica from Rice Husk for Zeolite Synthesis. Nigerian Journal of Basic and Applied Sciences. 24. 41. 10.4314/njbas.v24i1.7.

47. Shabir, Qurrat & Pokale, A. & Loni, Armando & Johnson, D. & Canham, Leigh & Fenollosa, Roberto & Tymczenko, M. & Rodriguez, Isabelle & Meseguer, Francisco & Cros, A. & Cantarero, Andres. (2011). Medically Biodegradable Hydrogenated Amorphous Silicon Microspheres. Silicon. 3. 10.1007/s12633-011-9097-4.

48. Chen, Fenghua & Yan, Fufeng & Chen, Qingtao & Wang, Yongwei & Han, Lifeng & Chen, Zhijun & Fang, Shaoming. (2014). Fabrication of Fe3O4@SiO2@TiO2 nanoparticles supported by graphene oxide sheets for the repeated adsorption and photocatalytic degradation of rhodamine B under UV irradiation. Dalton transactions (Cambridge, England: 2003). 43. 10.1039/c4dt01702a.

49. Bergmann, Carlos. (2015). Raman Spectroscopy of Iron Oxide of Nanoparticles (Fe3O4). Journal of Material Science & Engineering. 05. 10.4172/2169-0022.1000217.

50. Ian J. Bruce* and Tapas Sen. Surface Modification of Magnetic Nanoparticles with Alkoxysilanes and Their Application in Magnetic Bioseparations. Langmuir 2005, 21, 7029-7035.

51. LEE, Jun & LEE, Eun & HWANG, Hae. (2012). Synthesis of Fe3O4-coated silica aerogel nanocomposites. Transactions of Nonferrous Metals Society of China. 22. s702–s706. 10.1016/S1003-6326(12)61790-7.

52. Azadmanjiri, Jalal & Simon, George & Suzuki, Kiyonori & Selomulya, Cordelia & Cashion, John. (2011). Phase reduction of coated maghemite (g-Fe_2O_3) nanoparticles under microwave-induced plasma heating for rapid heat treatment. Journal of Materials Chemistry. 22. 617-625. 10.1039/c1jm12524a.

53. Han, Hongmei & Johnson, A. & Kaczor, J. & Kaur, Ms & Paszczynski, Andrzej & You, Qiang. (2010). Silica coated magnetic nanoparticles for separation of nuclear acidic waste. Journal of Applied Physics - J APPL PHYS. 107. 520-09. 10.1063/1.3358612.

54. Husnain, Syed & Um, Wooyong & Lee, Woojin & Chang, Yoon-Seok. (2018). Magnetite-based adsorbents for sequestration of radionuclides: A review. RSC Advances. 8. 2521-2540. 10.1039/C7RA12299C.

55. Kokate, Mangesh & Garadkar, Prof. K.M. & Gole, Anand. (2013). One pot synthesis of magnetite-silica nanocomposites: Applications as tags, entrapment matrix and in water purification. J. Mater. Chem. A. 1. 2022-2029. 10.1039/C2TA00951J.

56. Ahmad, M.K. & Islam, Shaumik & Rahman, M. & Haque, Md & Islam, Md. (2010). Heavy Metals in Water, Sediment and Some Fishes of Buriganga River, Bangladesh. International Journal of Environmental Research. 4. 321-332.

57. Hill, S.J. & Fisher, A.S.. (2016). Atomic Absorption, Methods and Instrumentation. 10.1016/B978-0-12-803224-4.00099-6.

58. Mokaddes, M.A.A. & Nahar, B.S. & Baten, M.A.. (2013). Status of Heavy Metal Contaminations of Lake Water of Dhaka Metropolitan City. Journal of Environmental Science and Natural Resources. 5. 10.3329/jesnr.v5i2.14841.

59. Ahmed, Minhaz & Matsumoto, Masaru & Kurosawa, Kiyoshi. (2018). Heavy Metal Contamination of Irrigation Water, Soil, and Vegetables in a Multi-industry District of Bangladesh. International Journal of Environmental Research. 12. 10.1007/s41742-018-0113-z.

60. Bhuyan, M.S., Bakar, M.A., Rashed-Un-Nabi, M. et al. Monitoring and assessment of heavy metal contamination in surface water and sediment of the Old Brahmaputra River, Bangladesh. Appl Water Sci 9, 125 (2019). https://doi.org/10.1007/s13201-019-1004-y.

61. Sobahni, Sarah. (2017). Network formation and thermal stability enhancement in evolutionary crosslinked PDMS elastomers with sol-gel-formed silica nanoparticles: Comparativeness between as-received and pre-hydrolyzed TEOS. Progress in Organic Coatings. 113. 117-125. 10.1016/j.porgcoat.2017.08.012.

62. Dang, Feng & Enomoto, Naoya & Hojo, Junichi & Enpuku, Keiji. (2009). Sonochemical coating of magnetite nanoparticles with silica. Ultrasonics sonochemistry. 17. 193-9. 10.1016/j.ultsonch.2009.05.013.

63. Yew, Yen Pin & Kamyar, Shameli & Miyake, Mikio & Khairudin, Nurul & Mohamad, Shaza & Hara, Hirofumi & Nordin, Mariam & Lee, Kar Xin. (2017). An Eco-Friendly Means of Biosynthesis of Superparamagnetic Magnetite Nanoparticles via Marine Polymer. IEEE Transactions on Nanotechnology. PP. 1-1. 10.1109/TNANO.2017.2747088.

64. Yuvakkumar, R., & Hong, S. I. (2014). Green Synthesis of Spinel Magnetite Iron Oxide Nanoparticles. Advanced Materials Research, 1051, 39-42 https://doi.org/10.4028/www.scientific.net/amr.1051.39.

65. Gautam, Ravindra & Sharma, Sanjay & Mahiya, Suresh & Chattopadhyaya, Mahesh. (2014). Heavy Metals In Water: Presence, Removal and Safety. https://doi.org/10.1039/9781782620174.

66. Karatapanis, A. E., Fiamegos, Y., & Stalikas, C. D. (2011). Silica-modified magnetic nanoparticles functionalized with cetylpyridinium bromide for the preconcentration of metals after complexation with 8-hydroxyquinoline. Talanta, *84*(3), 834–839. https://doi.org/10.1016/j.talanta.2011.02.013

67. Yi, Rong & Ye, Gang. (2019). Synthesis of core–shell magnetic titanate nanofibers composite for the efficient removal of Sr(ii). RSC Advances. 9. 27242-27249. 10.1039/C9RA06148G.

68. Yi, Rong & Ye, Gang & Fengcheng, Wu & Wen, Mingfen & Feng, Xiaogui. (2014). ChemInform Abstract: Highly Efficient Removal of 137 Cs in Seawater by Potassium Titanium Ferrocyanide Functionalized Magnetic Microspheres with Multilayer Core-Shell Structure.. RSC Adv.. 4. 10.1039/C4RA05397D.

69. Litvinenko Y.1 , Zabulonov Y.1 , Kadoshnikov V.1 , Yurzhenko M.2. Nanocomposite sio2/fe3o4 – a new material for radioactive waste compaction. International Conference "Nuclear Science and its Application", Samarkand, Uzbekistan, September 25-28, 2012.

70. Nayek, Chiranjib & Manna, Kaustuv & Bhattacharjee, Gourab & Murugavel, Pattukkannu & Obaidat, Ihab. (2017). Investigating Size- and Temperature-Dependent Coercivity and Saturation Magnetization in PEG Coated Fe_3O_4 Nanoparticles. Magnetochemistry. 3. 19. 10.3390/magnetochemistry3020019.

71. Li, Qing & Kartikowati, Christina & Horie, Shinji & Ogi, Takashi & Iwaki, Toru & Okuyama, Kikuo. (2017). Correlation between particle size/domain structure and magnetic properties of highly crystalline Fe3O4 nanoparticles. Scientific Reports. 7. 10.1038/s41598-017-09897-5.

72. Hu, Ping & Chang, Tian & Chen, Wen-Jing & Deng, Jie & Li, Shi-Lei & Zuo, Ye-Gai & Kang, Lu & Yang, Fan & Hostetter, Megan. (2018). Temperature effects on magnetic properties of Fe3O4 nanoparticles synthesized by the sol-gel explosion-assisted method. Journal of Alloys and Compounds. 773. 10.1016/j.jallcom.2018.09.238.

73. Kong, Ing & Ahmad, Sahrim & Abdullah, M. & Yusoff, Ahmad. (2009). The Effect Of Temperature On Magnetic Behavior Of Magnetite Nanoparticles And Its Nanocomposites. AIP Conference Proceedings. 1136. 830-834. 10.1063/1.3160267.

74. Bohra, Murtaza & Agarwal, Nishit & Singh, Vidyadhar. (2019). A Short Review on Verwey Transition in Nanostructured Fe_3O_4 Materials. Journal of Nanomaterials. 2019. 1-18. 10.1155/2019/8457383.

75. Pinki Singh, Manjari Shukla and Chandan Upadhyay. Signatures of consolidated superparamagnetic and spin-glass behavior in magnetite–silver core–shell nanoparticles. Nanoscale, 2018, 10, 22583.

76. Upadhyay, Sneha & Parekh, Kinnari & Pandey, Brajesh. (2016). Influence of crystallite size on the magnetic properties of Fe_3O_4 nanoparticles. Journal of Alloys and Compounds. 678. 10.1016/j.jallcom.2016.03.279.

77. Dhaliwal, S.S., Singh, J., Taneja, P.K. *et al.* Remediation techniques for removal of heavy metals from the soil contaminated through different sources: a review. Environ Sci Pollut Res **27,** 1319–1333 (2020). https://doi.org/10.1007/s11356-019-06967-1

78. Moni, S.A., Satter, G.S., Reza, A.H.M.S. *et al.* Hydrochemistry and Arsenic Contamination of Shallow Aquifers in Bidyananda and Nazimkhan Unions, Rajarhat Upazilla, Kurigram, Bangladesh. J Geol Soc India **94,** 395–404 (2019). https://doi.org/10.1007/s12594-019-1327-1.